Electronic Supporting Information

The Underappreciated Influence of Ancillary Halide on Metal-Ligand Proton Tautomerism

Anant Kumar Jain, Michael R. Gau, Patrick J. Carroll, and Karen I. Goldberg*

Department of Chemistry, University of Pennsylvania, Philadelphia, Pennsylvania 19104, United States

Corresponding Author

*kig@sas.upenn.edu

Table of Contents

General Methods

All experiments and manipulations were performed using standard Schlenk techniques under an argon or nitrogen atmosphere, or in a nitrogen filled glovebox (unless stated otherwise). Deuterated solvents were purchased from Cambridge Isotope Laboratories. Acetone-d_6 was degassed by three successive freeze-pump-thaw cycles and stored over molecular sieves inside of an inert glovebox. DCM-d_2 was refluxed overnight with CaH_2, vacuum transferred, and stored in a glovebox. Acetone was degassed by sparging using nitrogen for 30 minutes, followed by storage over molecular sieves in a glovebox. Diethyl ether, dichloromethane, and acetonitrile were dried by passage through activated alumina and molecular sieves columns under a stream of argon (a Grubb's type solvent purification system by JC Meyer Solvent Systems). $[Ir(coe)_2Cl]_2$ (coe = cyclooctene),[1] 2-(di-*tert*-butylphosphaneyl)-1*H*-imidazole (**LH**),[2] and $[Ir(coe)_2(acetone)_2][PF_6]$,[3] were synthesized following literature procedures. NEt_4Cl, NEt_4Br, NEt_4I, NMe_4F, NBu_4Br, NBu_4I, $(NBu_4)(PF_6)$, and 1,3,5-trimethoxybenzene were dried under vacuum prior to their use. NEt_3 was refluxed overnight with CaH_2, distilled, and stored over molecular sieves inside a glovebox. All other chemicals were used as received from commercial sources without further purification.

The NMR spectra were collected on a Bruker 400 or 500 MHz spectrometer at ambient probe temperatures. NMR tubes fitted with a J. Young style Teflon valve were used to obtain NMR data in inert atmosphere. ^1H, $^1H\{^{31}P\}$, $^1H\{^{19}F\}$ NMR spectral data are reported in ppm and were referenced to residual protons in the deuterated solvents: DCM-d_2 (5.32 ppm) and acetone-d_6 (2.05 ppm).[4] $^{13}C\{^1H\}$ NMR shifts were referenced to the solvent's signal: DCM-d_2 (53.84 ppm) and acetone-d_6 (29.84 ppm).[4] $^{31}P\{^1H\}$ NMR shifts were referenced to an 85% D_3PO_4 (in D_2O) external standard (0 ppm). ^{19}F and ^{19}F $\{^1H\}$ NMR shifts are reported relative to a fluorobenzene external standard (-113.15 ppm). IR spectra were taken on a PerkinElmer Spectrum 2000 FT-IR Spectrometer using a PerkinElmer IR liquid cell (NaCl). Accurate mass measurements were obtained on a Waters LCT Premier XE, time-of-flight, LCMS with electrospray ionization (ESI). The signals were mass measured against an internal lock mass reference of leucine enkephalin. Waters software calibrates the instruments, and reports measurements, by use of neutral atomic masses. Compositions of the samples for microanalysis were determined with a PerkinElmer 2400 Series II Analyzer at the CENTC Elemental Analysis Facility (University of Rochester). The samples were handled in inert conditions and combusted in a tin capsule that was crimp-sealed with a die apparatus.

Synthesis and Characterization of Complexes

Synthesis and Characterization of [^{LH}Ir][Cl]

Method 1:

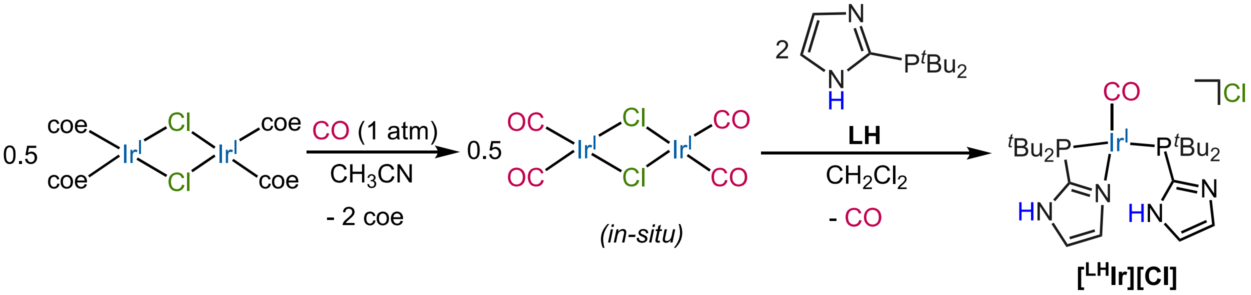

A suspension of [Ir(coe)$_2$Cl]$_2$ (205 mg, 0.228 mmol) in 50 mL of acetonitrile was prepared in a 100 mL Schlenk flask in an inert atmosphere glovebox. The flask was placed under an atmosphere of CO through its side arm (without degassing) for 10 minutes with constant stirring until the suspension turned homogenous. The resulting yellow-green solution indicative of the formation of [Ir(CO)$_2$Cl]$_2$ was brought back to an inert atmosphere on Schlenk line (no degassing). A solution of LH (193 mg, 0.910 mmol) in 16 mL dichloromethane was transferred *via* canula to the solution of [Ir(CO)$_2$Cl]$_2$, and the resulting mixture was stirred for 40 minutes to obtain a bright yellow homogeneous solution. Thereafter, the solvents were evaporated under vacuum at 30 °C for 2 hours and the yellow powder obtained was collected on a fine porosity glass fritted funnel. The powder was washed with 60 mL diethyl ether and dried under vacuum.

Yield: 261 mg (84%).

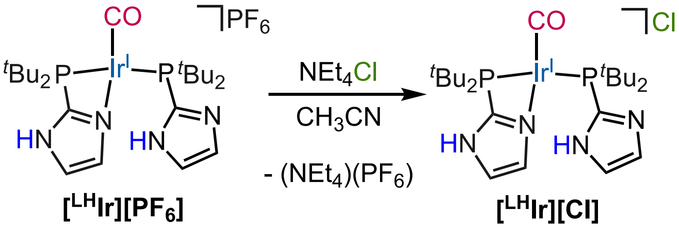

Method 2:

[^{LH}Ir][Cl] can also be prepared by performing a salt-metathesis reaction of **[^{LH}Ir][PF$_6$]** (synthesis described below) with NEt$_4$Cl. **[^{LH}Ir][PF$_6$]** (254 mg, 0.321 mmol) and NEt$_4$Cl (53.4 mg, 0.323

mmol) were weighed in two separate vials. NEt_4Cl was dissolved in approximately 2 mL of acetonitrile and this solution was transferred to the vial containing **[^{LH}Ir][PF$_6$]**. The resulting solution was stirred for a minute resulting in a precipitation of the product. An additional 8 mL of acetonitrile was added to reaction mixture along the sides of the vial and the precipitate was allowed to settle for 5 minutes. The yellow precipitate (product) was then isolated by filtering the solution over a medium porosity glass fritted funnel, washing with 5 mL acetonitrile, and drying under vacuum. Single crystals suitable for X-ray diffraction were grown by preparing a saturated acetonitrile solution of the product **[^{LH}Ir][Cl]** at room temperature, and then storing it at -30 °C overnight.

Yield: 153 mg (84%).

Note: The product can be washed with more acetonitrile at the expense of yield if NMR spectral signals for $(NEt_4)(PF_6)$ are present.

<u>CAUTION:</u> Experiments involving CO gas must be performed in a well-ventilated and working fume hood with utmost care to avoid any inhalation of the toxic gas.

As described in the main text, when solid **[^{LH}Ir][Cl]** is dissolved in DCM-d_2, spectral signals corresponding to both ionic **[^{LH}Ir][Cl]** species and the neutral hydridic **[H–^{L}Ir–Cl]** species are observed. NMR spectral signals corresponding to the ionic **[^{LH}Ir][Cl]** species have been assigned by comparison to the **[^{LH}Ir][PF$_6$]** spectral signals (see below for characterization of **[^{LH}Ir][PF$_6$]**). Remaining signals have been assigned to the neutral hydridic **[H–^{L}Ir–Cl]** species. Reader is cautioned that the spectral signals corresponding to **[H–^{L}Ir–Cl]** could not be fully resolved due to its low concentration as well as overlapping signals with **[^{LH}Ir][Cl]** species. The equilibrium constant (K_{eq}) value is provided on page S52.

^{1}H NMR (400 MHz, DCM-d_2): *(Signals corresponding to* **[^{LH}Ir][Cl]***)* δ 12.24 (br, 1H), 9.56 (br, 1H), 7.37 (s, 1H), 7.19 (s, 1H), 6.82 (s, 1H), 5.35 (s, 1H), 1.52 (d, $^3J_{P–H}$ = 16 Hz, 36H). *(Signals corresponding to* **[H–^{L}Ir–Cl]***)* δ 7.27, 7.19 (shoulder), 1.58, -17.22 (t, $^2J_{P–H}$ = 12 Hz).

^{31}P{^{1}H} NMR (162 MHz, DCM-d_2): *(Signals corresponding to* **[^{LH}Ir][Cl]***)* δ 50.11 (d, $^2J_{P–P}$ = 250 Hz), 38.56 (d, $^2J_{P–P}$ = 254 Hz).

^{13}C{^{1}H} NMR (126 MHz, DCM-d_2): *(Signals corresponding to* **[^{LH}Ir][Cl]***)* δ 177.44 (t, *J* couldn't be resolved), 153.32 (d, $^1J_{P–C}$ = 43 Hz), 139.77 (d, $^1J_{P–C}$ = 62 Hz), 131.18 (d, *J* couldn't be resolved), 127.35 (d, $^3J_{P–C}$ = 11 Hz), 121.82 (br), 119.16 (br), 38.59 (d, $^1J_{P–C}$ = 25 Hz), 35.84 (d,

$^1J_{\text{P–C}}$ = 18 Hz), 30.18 (br). *(Signals corresponding to* **[H–$^{\mathbf{L}}$Ir–Cl]***)* δ 142.28 (t, *J* couldn't be resolved), 129.72 (t, $J_{\text{P–C}}$ = 5 Hz), 128.81 (br), 119.33 (s), 118.75 (br), 42.57 (br), 40.19 (t, $J_{\text{P–C}}$ = 14 Hz), 38.99 (t, $J_{\text{P–C}}$ = 13 Hz), 31.06 (s), 30.86 (br).

IR (ν_{co} *corresponding to* **[$^{\mathbf{LH}}$Ir][Cl]**, DCM-d_2): 1967 cm^{-1}

Accurate Mass Measurement (ESI+, TOF) $C_{23}H_{42}IrN_4OP_2$ *(Corresponding to* **[$^{\mathbf{LH}}$Ir][Cl]***)*: Theoretical Mass = 645.2463, Observed Mass = 645.2473.

Anal. Calcd. For **[$^{\mathbf{LH}}$Ir][Cl]**, $C_{23}H_{42}ClIrN_4OP_2$: C, 40.61; H, 6.22; N, 8.24. Found: C, 40.15; H, 5.99; N, 8.10.

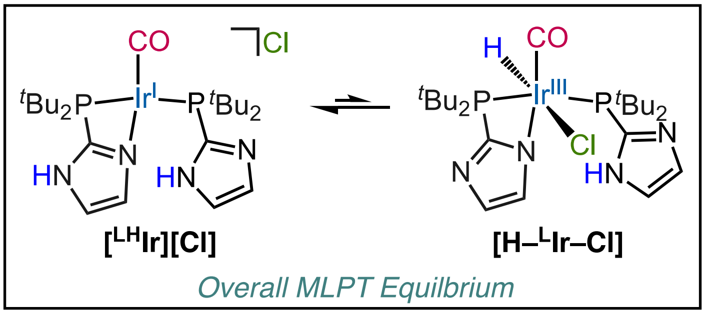

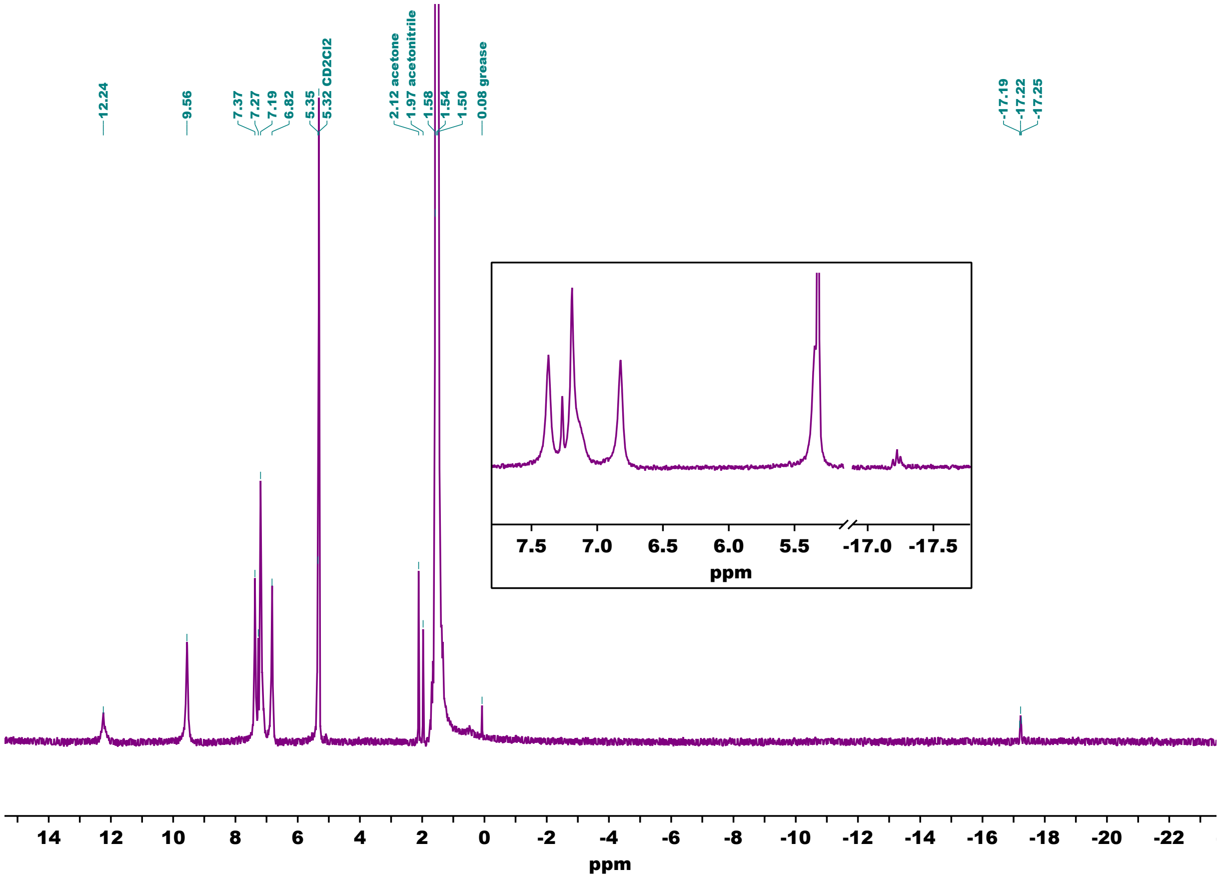

Figure S1. ^{1}H NMR (400 MHz, DCM-d_2) spectrum of **[^{LH}Ir][Cl]**.

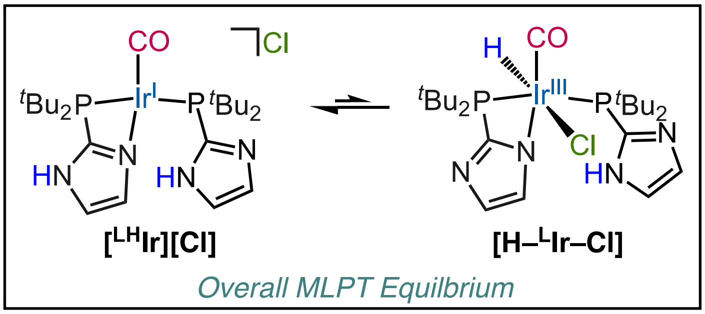

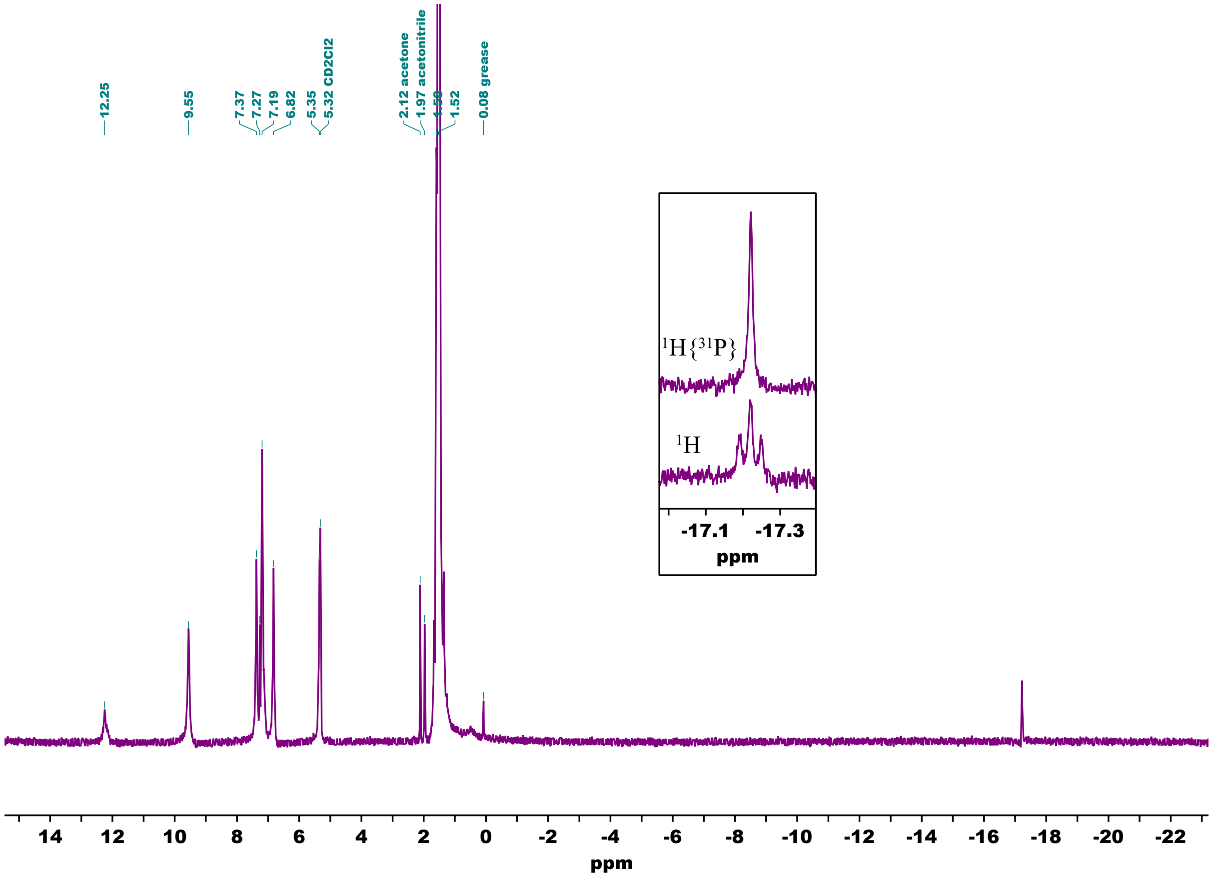

Figure S2. $^{1}H\{^{31}P\}$ NMR (400 MHz, DCM-d_2) spectrum of **[^{LH}Ir][Cl]**. (Inset) Ir–H resonance in the ^{1}H and $^{1}H\{^{31}P\}$ NMR spectrum.

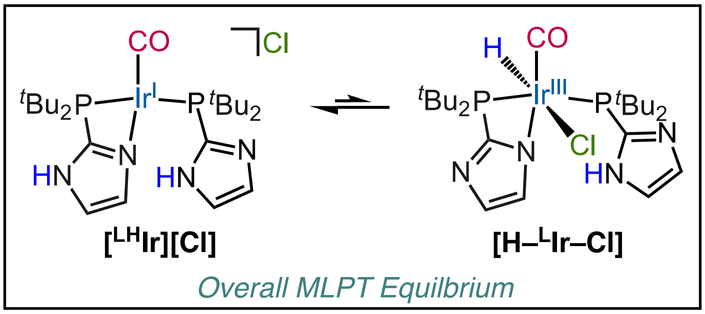

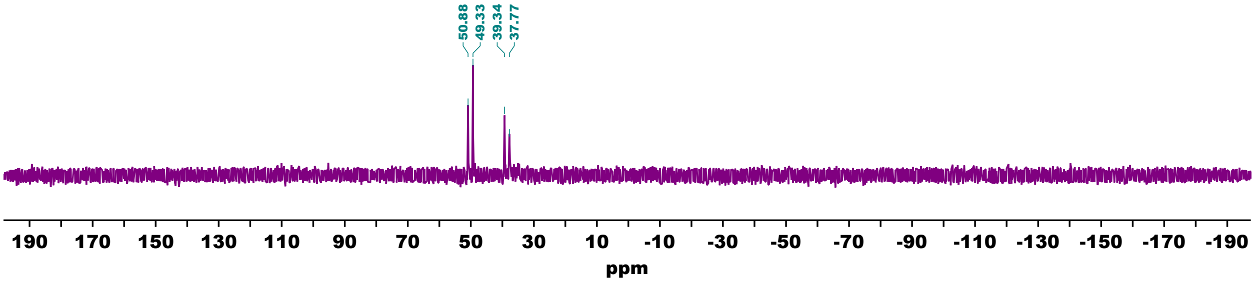

Figure S3. $^{31}P\{^{1}H\}$ NMR (162 MHz, DCM-d_2) spectrum of **[^{LH}Ir][Cl]**.

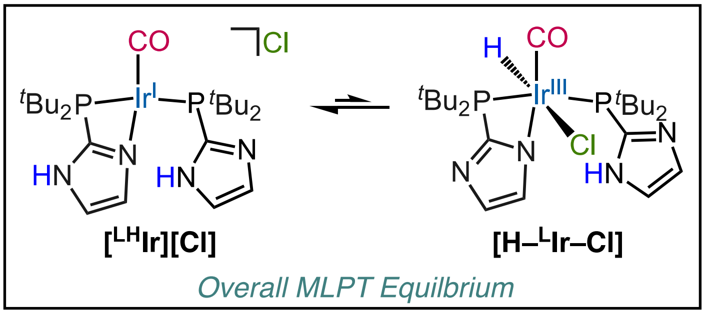

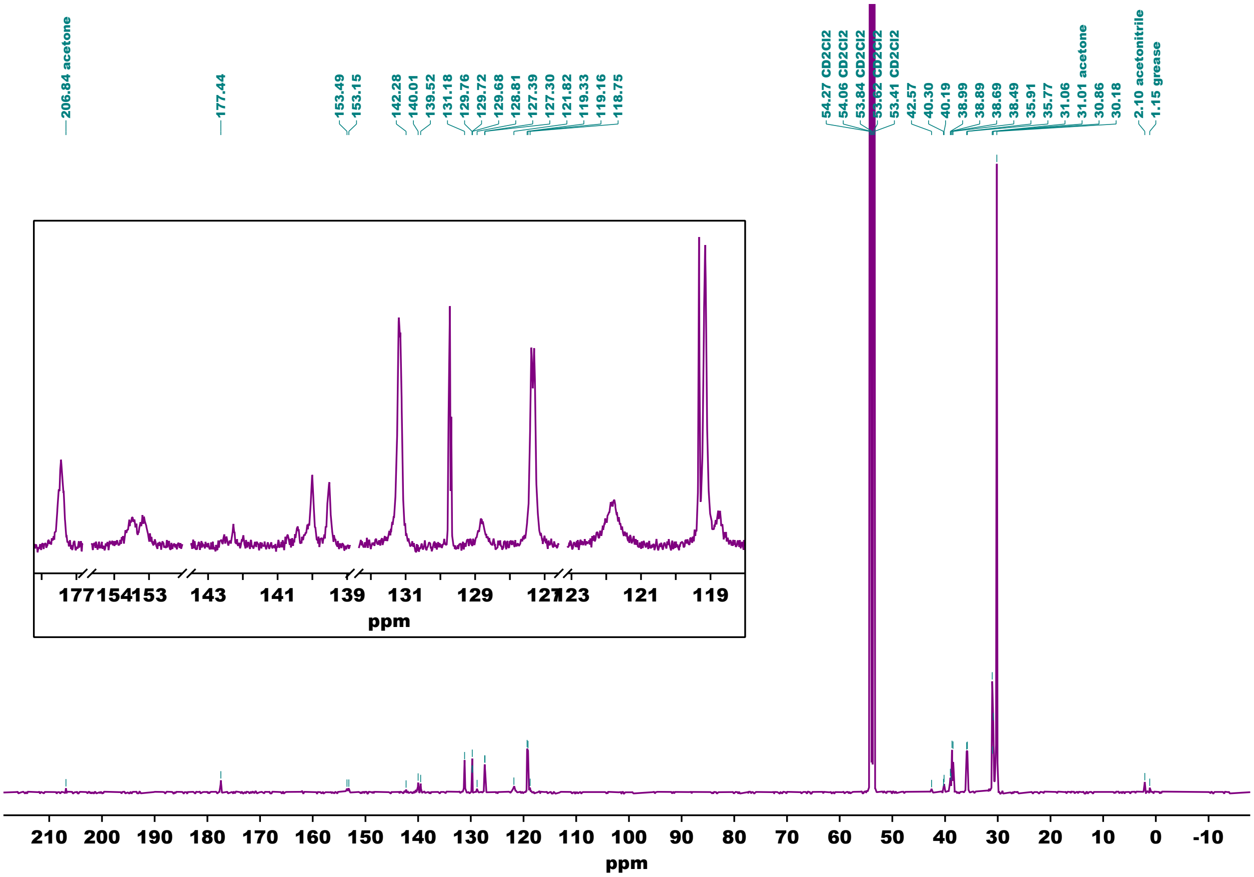

Figure S4. $^{13}C\{^1H\}$ NMR (126 MHz, DCM-d_2) spectrum of **[^{LH}Ir][Cl]**.

Synthesis and Characterization of Ir-1

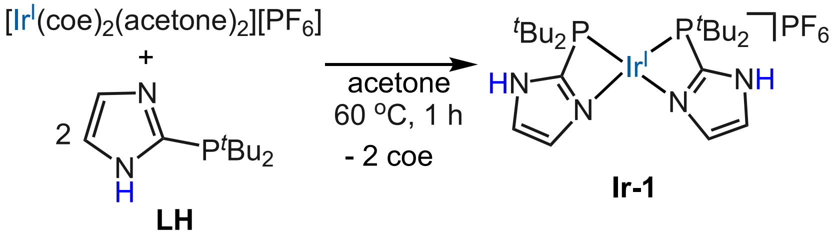

$[Ir(coe)_2(acetone)_2][PF_6]$ (62.9 mg, 0.093 mmol) and LH (41.3 mg, 0.194 mmol) were weighed in two separate vials. 5 mL acetone (enough to dissolve) was added to each vial. Using a pipette, the solution of $[Ir(coe)_2(acetone)_2][PF_6]$ was added to the solution of LH. The resulting mixture was transferred to a (large) J. Young style tube and heated at 60 °C for an hour. Then, the reaction mixture was concentrated to approximately 1 mL volume. Addition of 10 mL diethyl ether to the concentrated solution caused precipitation of the product **Ir-1** which was filtered and collected on a fine porosity glass fritted funnel. The orange solid obtained was then washed with 10 mL diethyl ether and dried under vacuum. Single crystals suitable for X-ray diffraction were grown overnight by vapor diffusion of an acetone solution of **Ir-1** with diethyl ether. **Ir-1** was found to be extremely sensitive to air as a solid as well as in solution.

Yield: 72 mg (97%).

^{1}H NMR (400 MHz, acetone-d_6): δ 12.49 (br, 2H), 7.77 (s, 2H), 7.23 (s, 2H), 1.49 (d, $^{3}J_{\mathrm{P-H}} = 12$ Hz, 36 H).

^{31}P{^{1}H} NMR (162 MHz, acetone-d_6): δ 28.91 (s), -142.91 (sept, $^{1}J_{\mathrm{P-F}} = 708$ Hz).

^{13}C{^{1}H} NMR (126 MHz, acetone-d_6): δ 158.72 (d, $^{1}J_{\mathrm{P-C}} = 25$ Hz), 129.28 (t, $^{3}J_{\mathrm{P-C}} = 8$ Hz), 118.95 (s), 33.16 (m), 30.02 (m, signals overlapping with those of acetone-d_6).

Accurate Mass Measurement (ESI+, TOF) $C_{22}H_{42}IrN_4P_2$: Theoretical Mass = 615.2491, Observed Mass = 615.2499 (^{191}Ir measured).

Anal. Calcd. For **Ir-1** (+ H_2O), $C_{22}H_{44}F_6IrN_4OP_3$: C, 33.89; H, 5.69; N, 7.19. Found: C, 33.97; H, 5.51; N, 7.29.

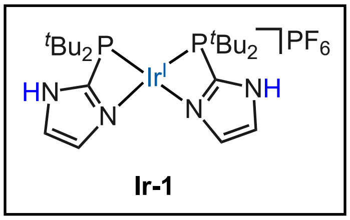

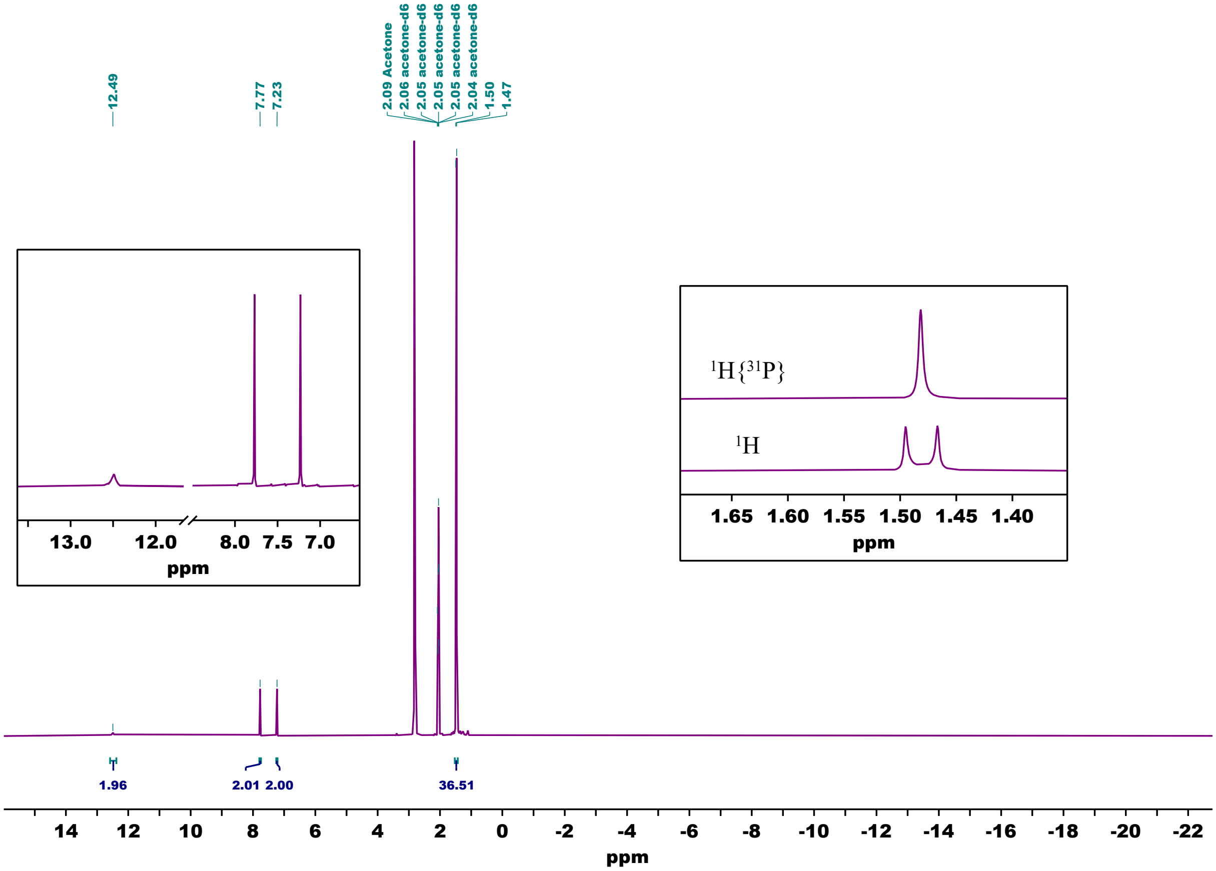

Figure S5. ^{1}H NMR (500 MHz, acetone-d_6) spectrum of **Ir-1**. (Right Inset) Aliphatic region of the ^{1}H and ^{1}H{^{31}P} NMR spectrum.

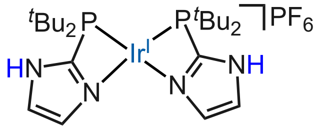

Ir-1

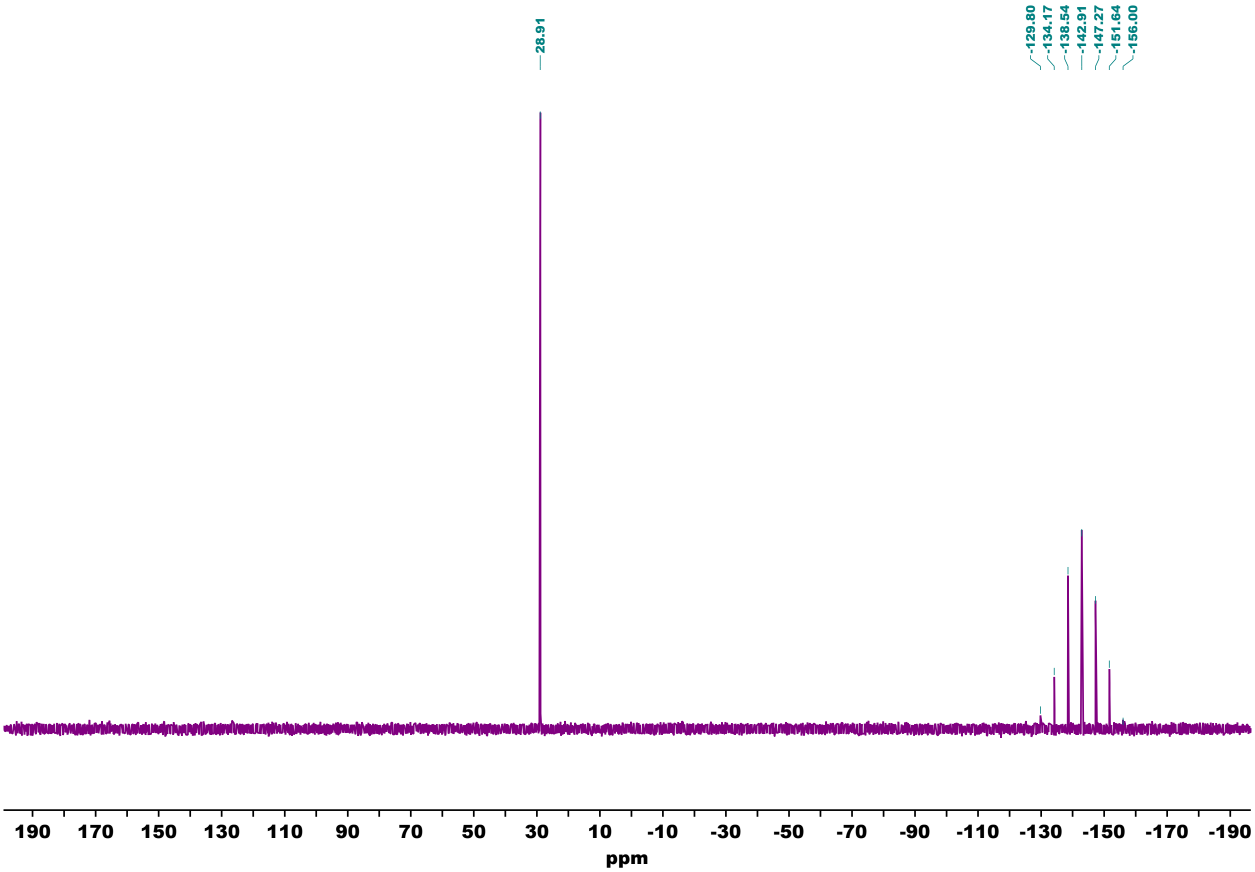

Figure S6. ^{31}P{^{1}H} NMR (162 MHz, acetone-d_6) spectrum of **Ir-1**.

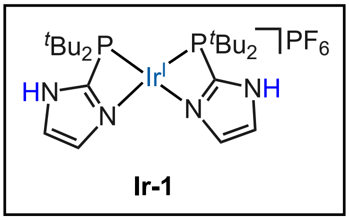

Ir-1

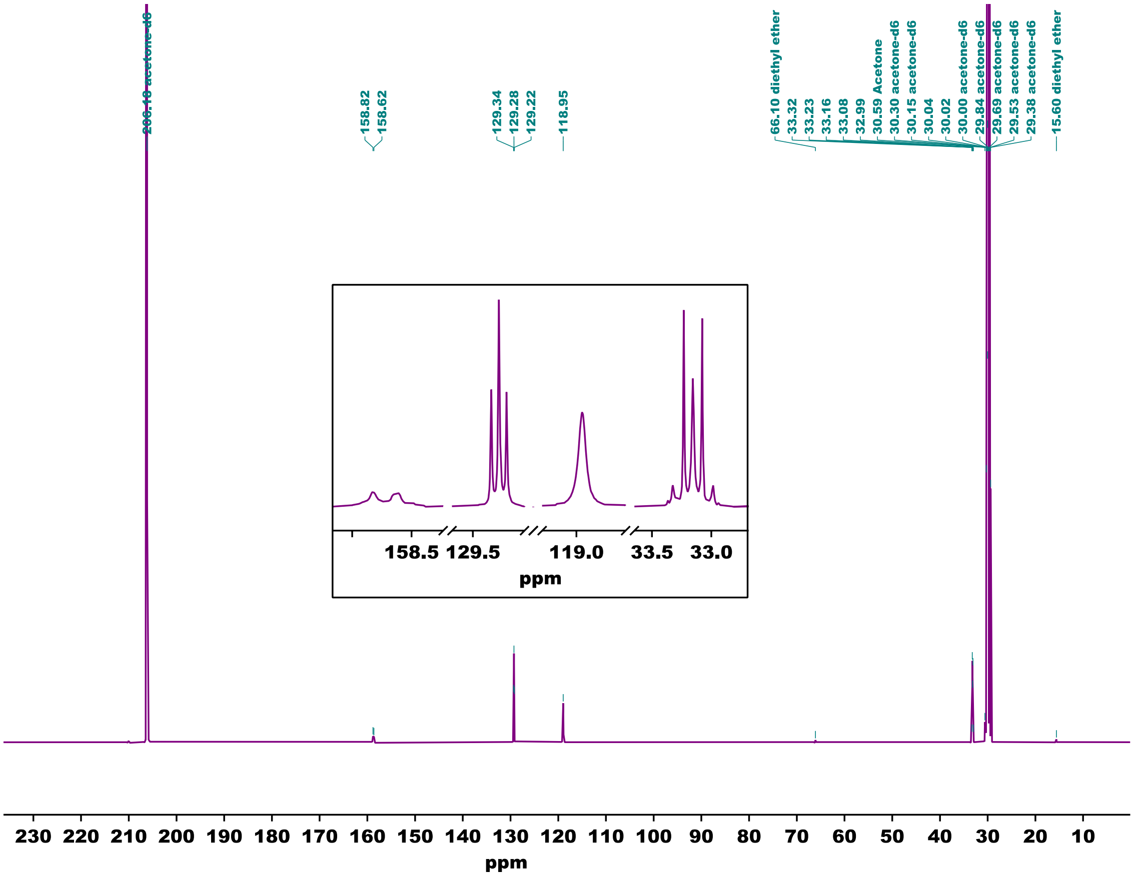

Figure S7. ^{13}C{^{1}H} NMR (126 MHz, acetone-d_6) spectrum of **Ir-1**.

Synthesis and Characterization of [^{LH}Ir][PF$_6$]

Method 1:

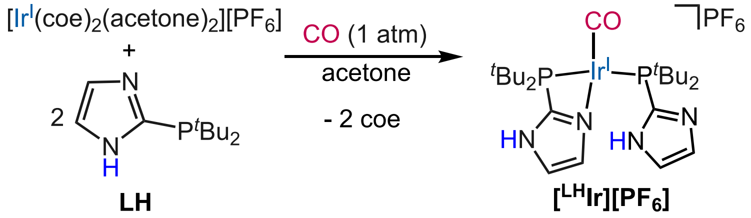

[Ir(coe)$_2$(acetone)$_2$][PF$_6$] (470 mg, 0.698 mmol) and LH (296 mg, 1.39 mmol) were weighed in two separate vials in an inert glovebox. 12 mL acetone (enough to dissolve) was added to each vial, and both solutions were transferred to a 50 mL Schlenk flask. The flask was placed under an atmosphere of CO through its side arm (without degassing) for 5 minutes resulting in a light-yellow color solution. The reaction mixture was then concentrated to 5 mL total volume using vacuum on a Schlenk line. (The steps described next can be performed in air) Addition of 40 mL diethyl ether to the concentrated solution caused precipitation of the product **[^{LH}Ir][PF$_6$]** which was filtered and collected on a fine porosity glass fritted funnel. The yellow solid was then washed with 30 mL diethyl ether and dried under vacuum. Single crystals suitable for X-ray diffraction were grown overnight by vapor diffusion of an acetone solution of **[^{LH}Ir][PF$_6$]** with diethyl ether.

Yield: 492 mg (89%).

Method 2:

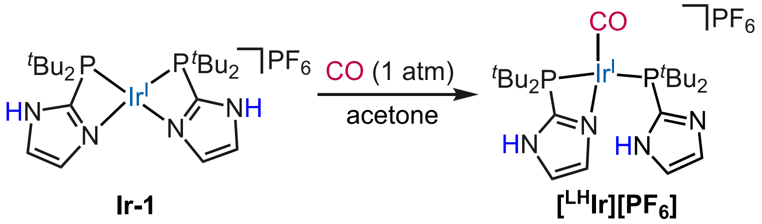

Alternatively, **[^{LH}Ir][PF$_6$]** was also prepared in similar yield by exposing an acetone solution of **Ir-1** to CO for 5 minutes and working up as described above.

CAUTION: Experiments involving CO gas must be performed in a well-ventilated and working fume hood with utmost care to avoid any inhalation of the toxic gas.

^{1}H NMR (400 MHz, DCM-d_2): δ 11.37 (br, 1H), 9.20 (br, 1H), 7.40 (s, 1H), 7.21 (s, 1H), 6.94 (s, 1H), 5.37 (s, 1H), 1.50 (d, $^3J_{P-H}$ = 16 Hz, 36H).

^{31}P{^{1}H} NMR (162 MHz, DCM-d_2): δ 49.80 (d, $^2J_{P-P}$ = 249 Hz), 38.97 (d, $^2J_{P-P}$ = 251 Hz), -143.84 (sept, $^1J_{P-F}$ = 713 Hz).

^{13}C{^{1}H} NMR (126 MHz, DCM-d_2): δ 176.10 (t, $^2J_{P-C}$ = 10 Hz), 153.04 (d, $^1J_{P-C}$ = 33 Hz), 139.44 (d, $^1J_{P-C}$ = 62 Hz), 131.48 (d, $^3J_{P-C}$ = 8 Hz), 127.88 (d, $^3J_{P-C}$ = 11 Hz), 121.46 (s), 119.30 (s), 38.75 (d, $^1J_{P-C}$ = 25 Hz), 36.00 (d, $^1J_{P-C}$ = 16 Hz), 30.22 (s), 29.86 (s).

IR (ν_{co}, DCM-d_2): 1973 cm^{-1}

Accurate Mass Measurement (ESI+, TOF) $C_{23}H_{42}IrN_4OP_2$: Theoretical Mass = 645.2463, Observed Mass = 645.2456.

Anal. Calcd. For **[$^{\mathbf{LH}}$Ir][PF$_6$]**, $C_{23}H_{42}F_6IrN_4OP_3$: C, 34.98; H, 5.36; N, 7.09. Found: C, 34.91; H, 5.02; N, 6.97.

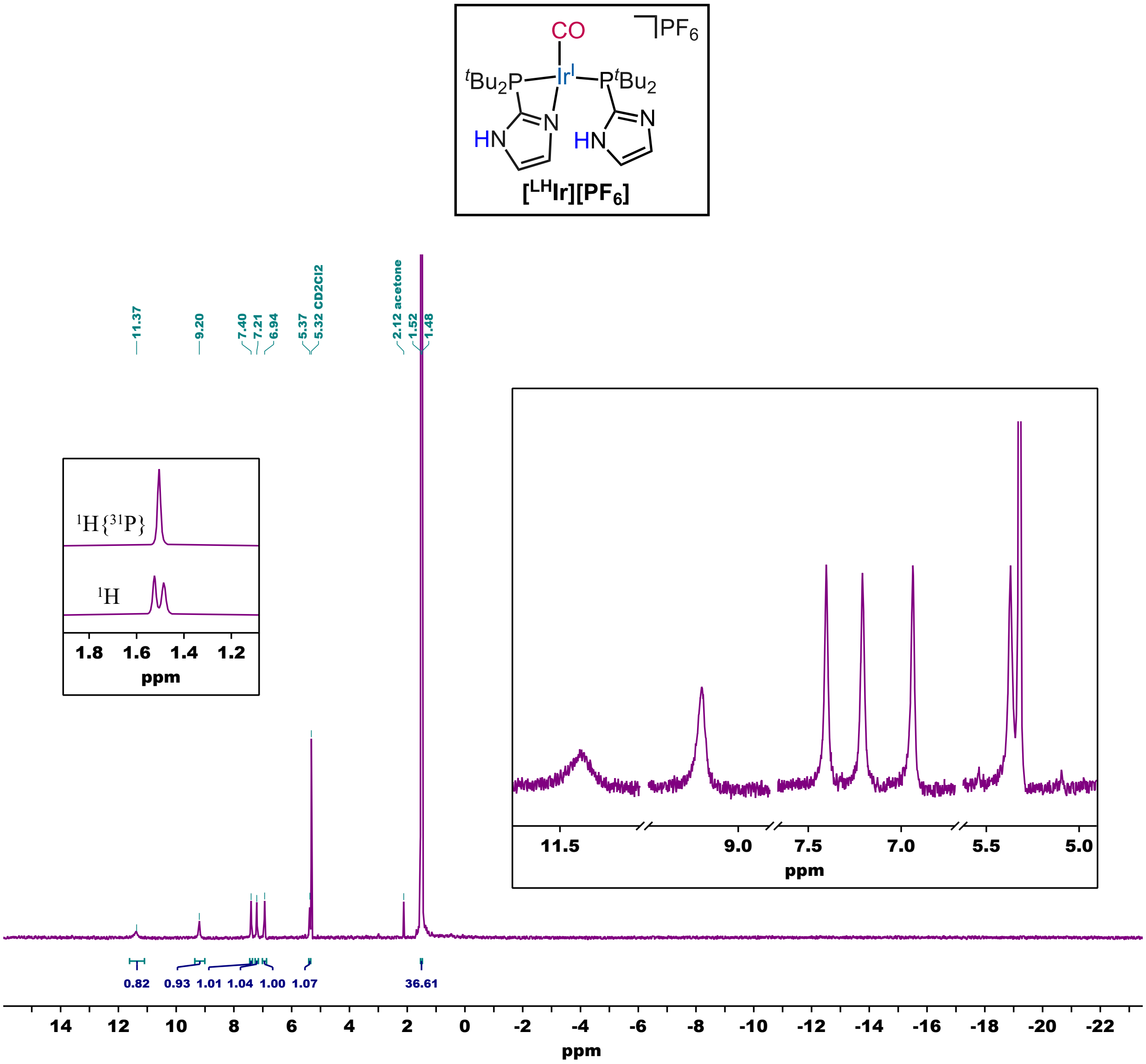

Figure S8. ^{1}H NMR (400 MHz, DCM-d_2) spectrum of **[^{LH}Ir][PF$_6$]**. (Left Inset) Aliphatic region of the ^{1}H and ^{1}H{^{31}P} NMR spectrum.

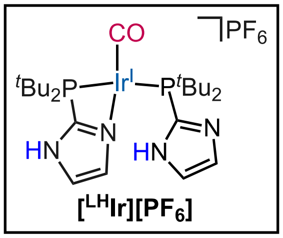

[^{LH}Ir][PF$_6$]

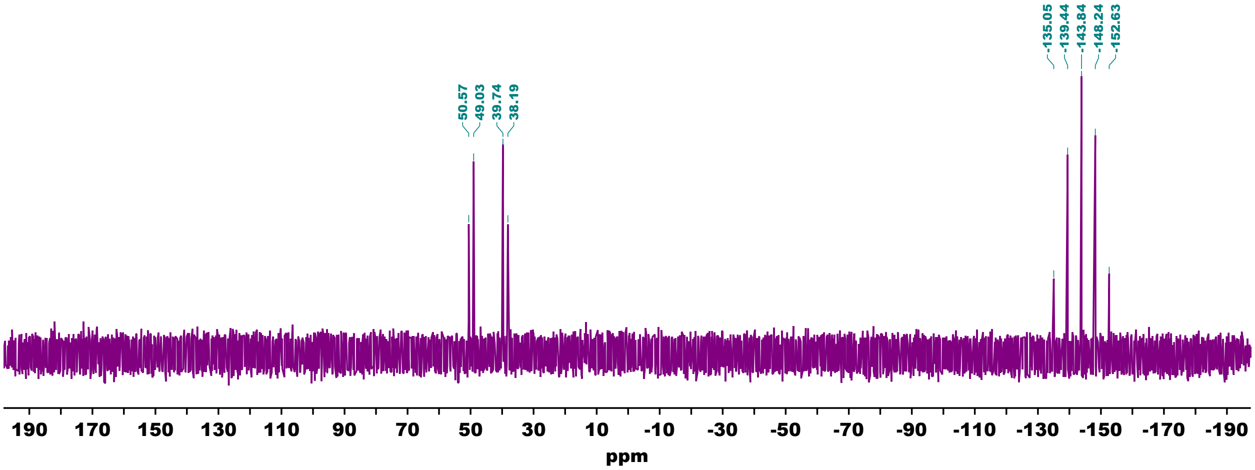

Figure S9. $^{31}P\{^1H\}$ NMR (162 MHz, DCM-d_2) spectrum of **[^{LH}Ir][PF$_6$]**.

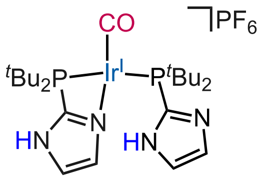

[^{LH}Ir][PF$_6$]

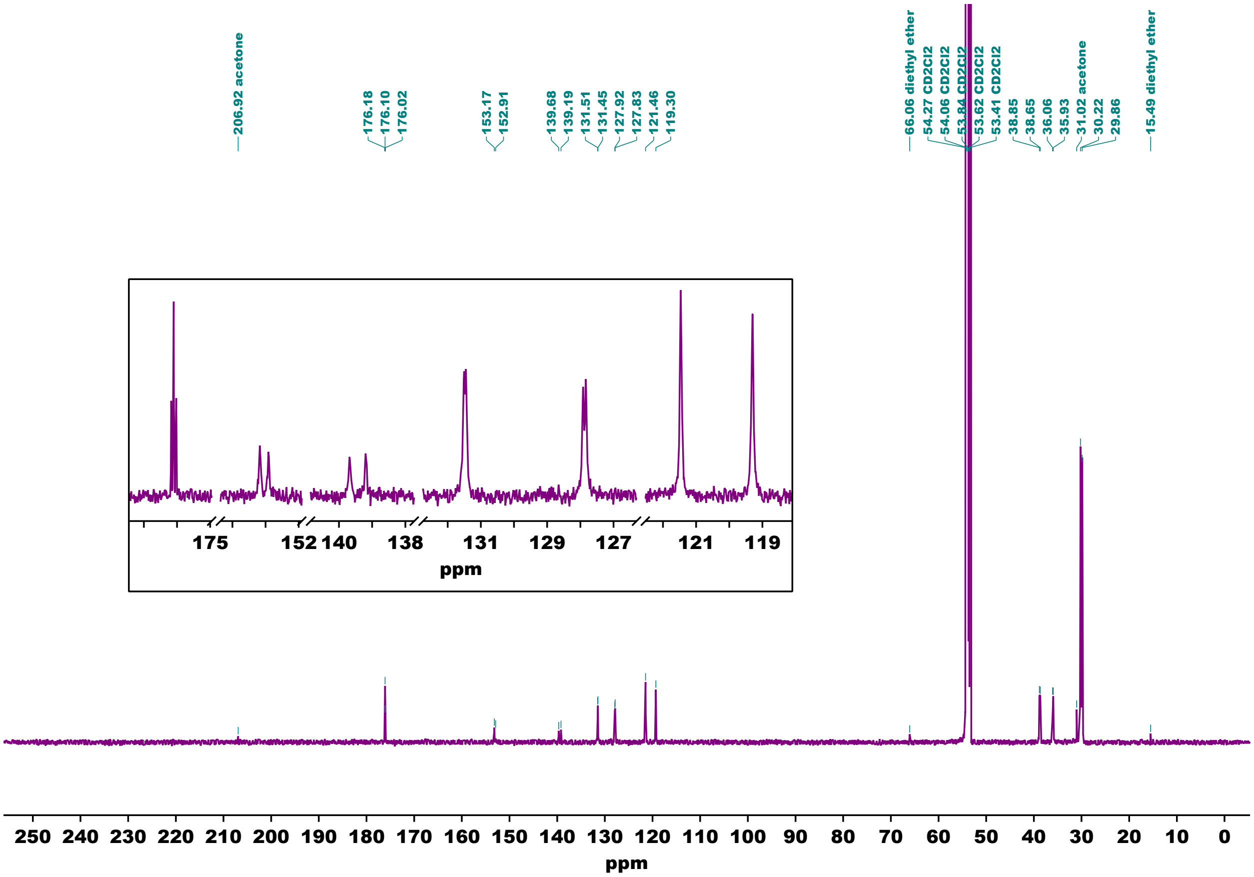

Figure S10. $^{13}C\{^1H\}$ NMR (126 MHz, DCM-d_2) spectrum of **[^{LH}Ir][PF$_6$]**.

Synthesis and Characterization of [$^{\mathbf{LH}}$Ir][Br]

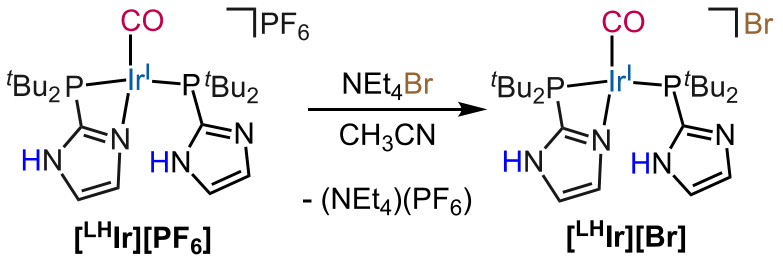

[$^{\mathbf{LH}}$Ir][PF$_6$] (194 mg, 0.246 mmol) and NEt$_4$Br (51.9 mg, 0.233 mmol) were weighed in two separate vials. 4 mL of acetonitrile (enough to dissolve) was added to both vials, and the solution of NEt$_4$Br was transferred to the solution of **[$^{\mathbf{LH}}$Ir][PF$_6$]** and stirred vigorously. The product **[$^{\mathbf{LH}}$Ir][Br]** started precipitating out of solution within few minutes, and at this point the stirring was stopped and the precipitate was allowed to settle for 5 minutes. The yellow precipitate (product) was then isolated by filtering the solution over a medium porosity glass fritted funnel, washing with 3 mL acetonitrile, and drying under vacuum. Single crystals suitable for X-ray diffraction were grown by preparing a saturated acetonitrile solution of the product **[$^{\mathbf{LH}}$Ir][Br]** at room temperature, and then storing it at -30 °C overnight.
Yield: 143 mg (81%).
Note: The product can be washed with more acetonitrile or DCM at the expense of some of the yield if NMR spectral signals for (NEt$_4$)(PF$_6$) are present.

^{1}H NMR (400 MHz, DCM-d_2): δ 15.40 (br, 1H), 9.28 (br, 1H), 7.39 (s, 1H), 7.18 (s, 1H), 6.90 (s, 1H), 5.35 (s, 1H), 1.53 (two overlapping d, 36H).

^{31}P{^{1}H} NMR (162 MHz, DCM-d_2): δ 50.07 (d, $^2J_{\mathrm{P-P}} = 253$ Hz), 39.72 (d, $^2J_{\mathrm{P-P}} = 253$ Hz).

^{13}C{^{1}H} NMR (126 MHz, DCM-d_2): δ 176.93 (t, $^2J_{\mathrm{P-C}} = 9$ Hz), 152.54 (d, $^1J_{\mathrm{P-C}} = 38$ Hz), 139.70 (d, $^1J_{\mathrm{P-C}} = 60$ Hz), 131.34 (d, $^3J_{\mathrm{P-C}} = 8$ Hz), 127.33 (d, $^3J_{\mathrm{P-C}} = 10$ Hz), 120.84 (s), 119.12 (s), 38.63 (d, $^1J_{\mathrm{P-C}} = 25$ Hz), 35.93 (d, $^1J_{\mathrm{P-C}} = 18$ Hz), 30.23 (s), 30.19 (s).

IR (ν_{co}, DCM-d_2): 1969 cm^{-1}

Accurate Mass Measurement (ESI+, TOF) $C_{23}H_{42}IrN_4OP_2$: Theoretical Mass = 645.2463, Observed Mass = 645.2479.
Anal. Calcd. For **[$^{\mathbf{LH}}$Ir][Br]**, $C_{23}H_{42}BrIrN_4OP_2$: C, 38.12; H, 5.84; N, 7.73. Found: C, 37.87; H, 5.65; N, 7.83.

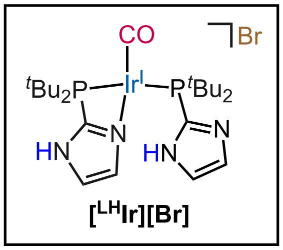

[^{LH}Ir][Br]

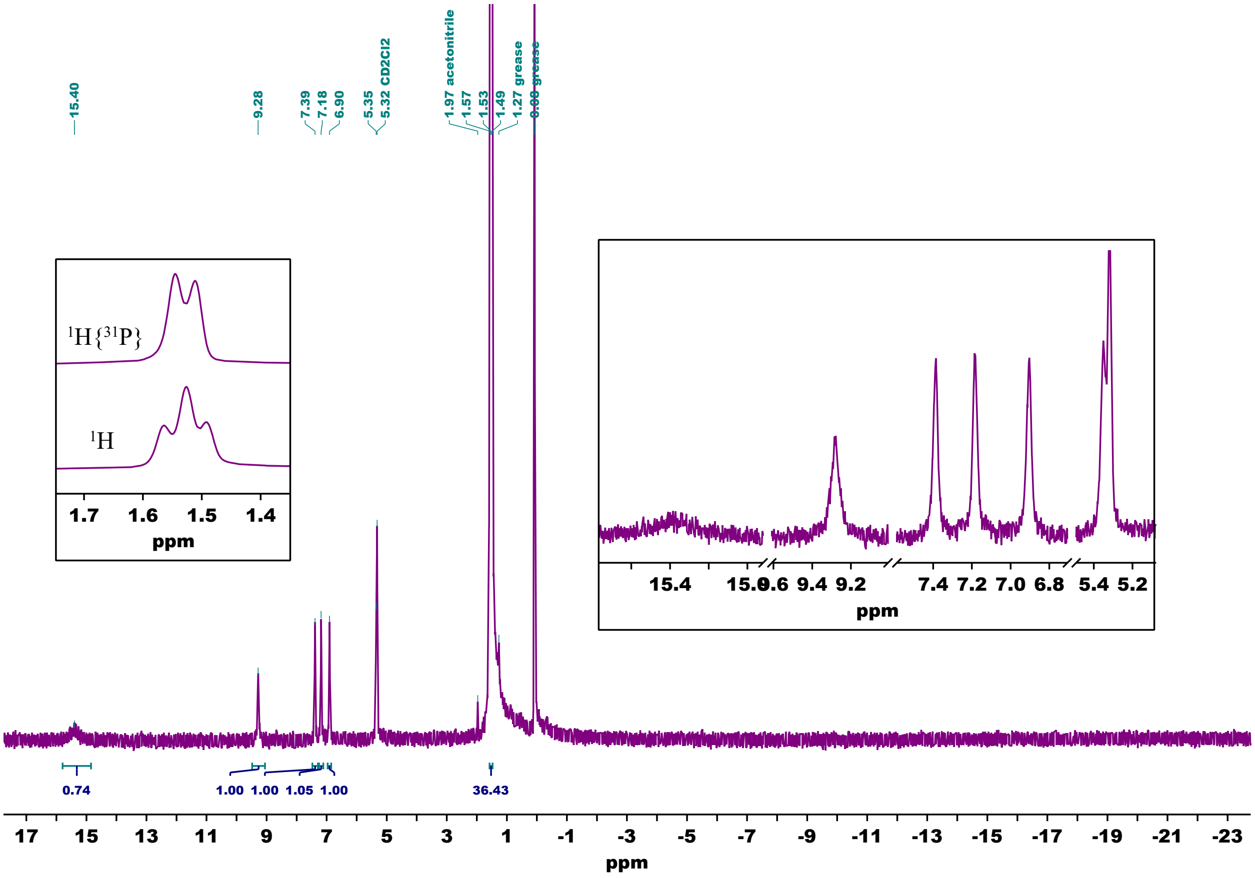

Figure S11. ^{1}H NMR (400 MHz, DCM-d_2) spectrum of **[^{LH}Ir][Br]**. (Left Inset) Aliphatic region of the ^{1}H and ^{1}H{^{31}P} NMR spectrum.

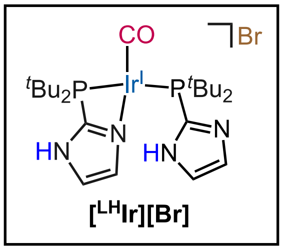

Figure S12. ^{31}P{^{1}H} NMR (162 MHz, DCM-d_2) spectrum of **[^{LH}Ir][Br]**.

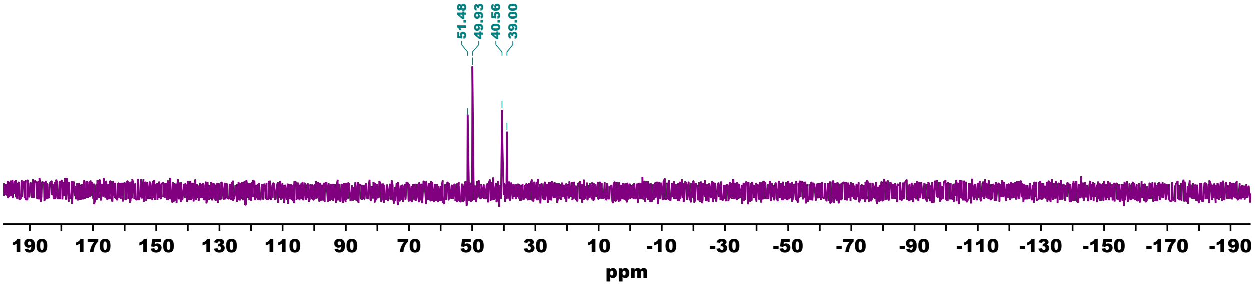

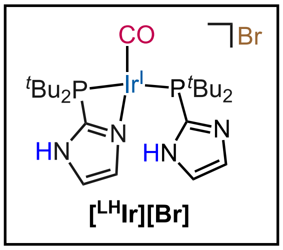

[^{LH}Ir][Br]

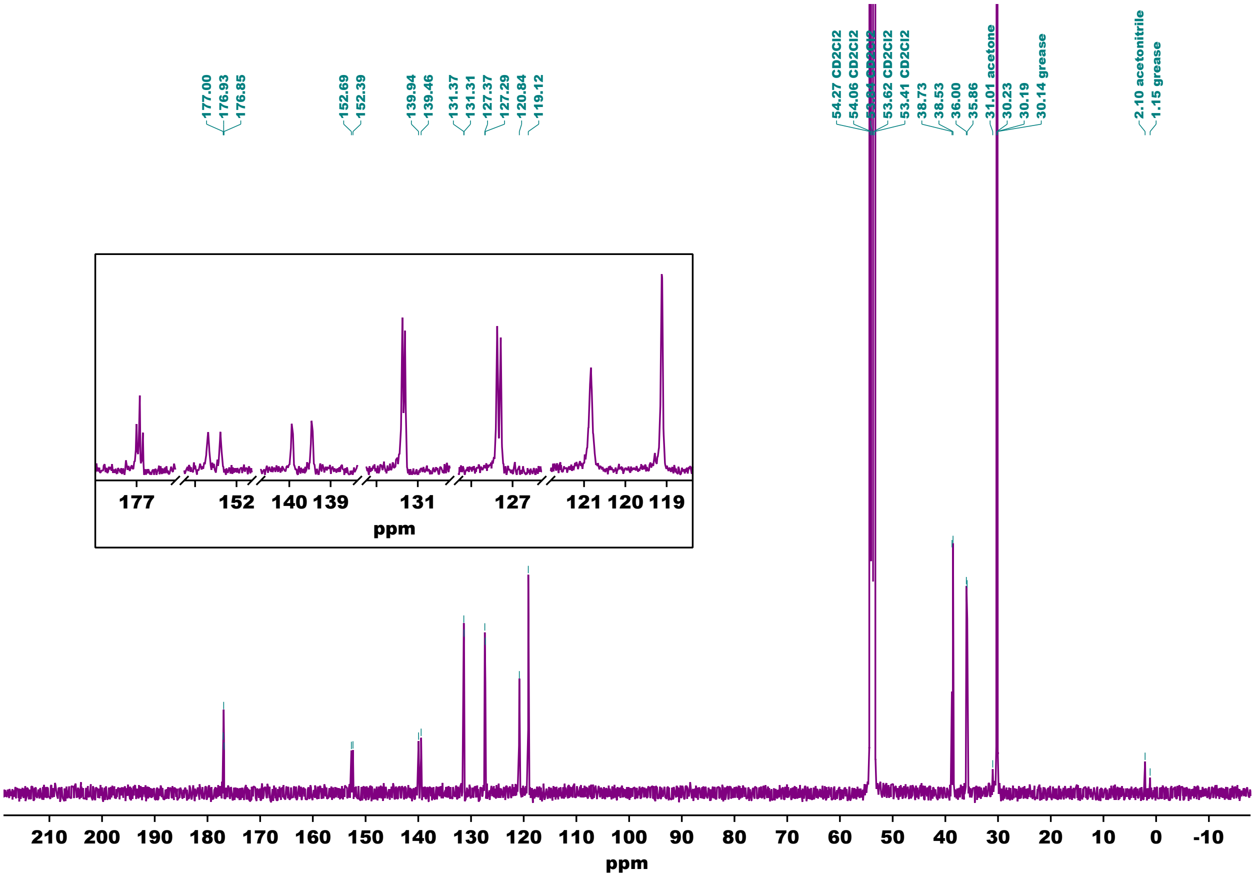

Figure S13. ^{13}C{^{1}H} NMR (126 MHz, DCM-d_2) spectrum of **[^{LH}Ir][Br]**.

Heating a DCM-d_2 solution of [$^{\mathbf{LH}}$Ir][Br]

3.00 mg (4.13×10^{-3} mmol) of **[$^{\mathbf{LH}}$Ir][Br]** was dissolved in 0.40 mL DCM-d_2 inside a glovebox. The solution was transferred to a J. Young NMR tube and then heated at 60 °C for 7 days. The calculated K_{eq} value is provided below on page S52.

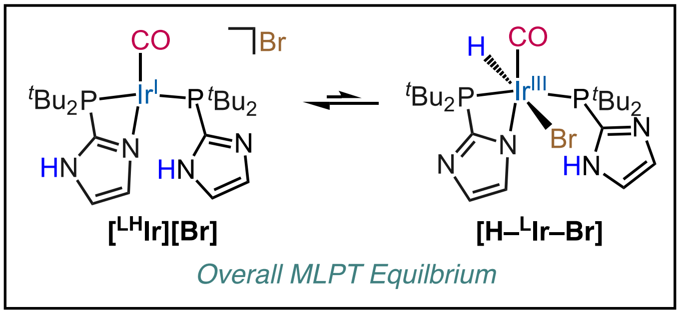

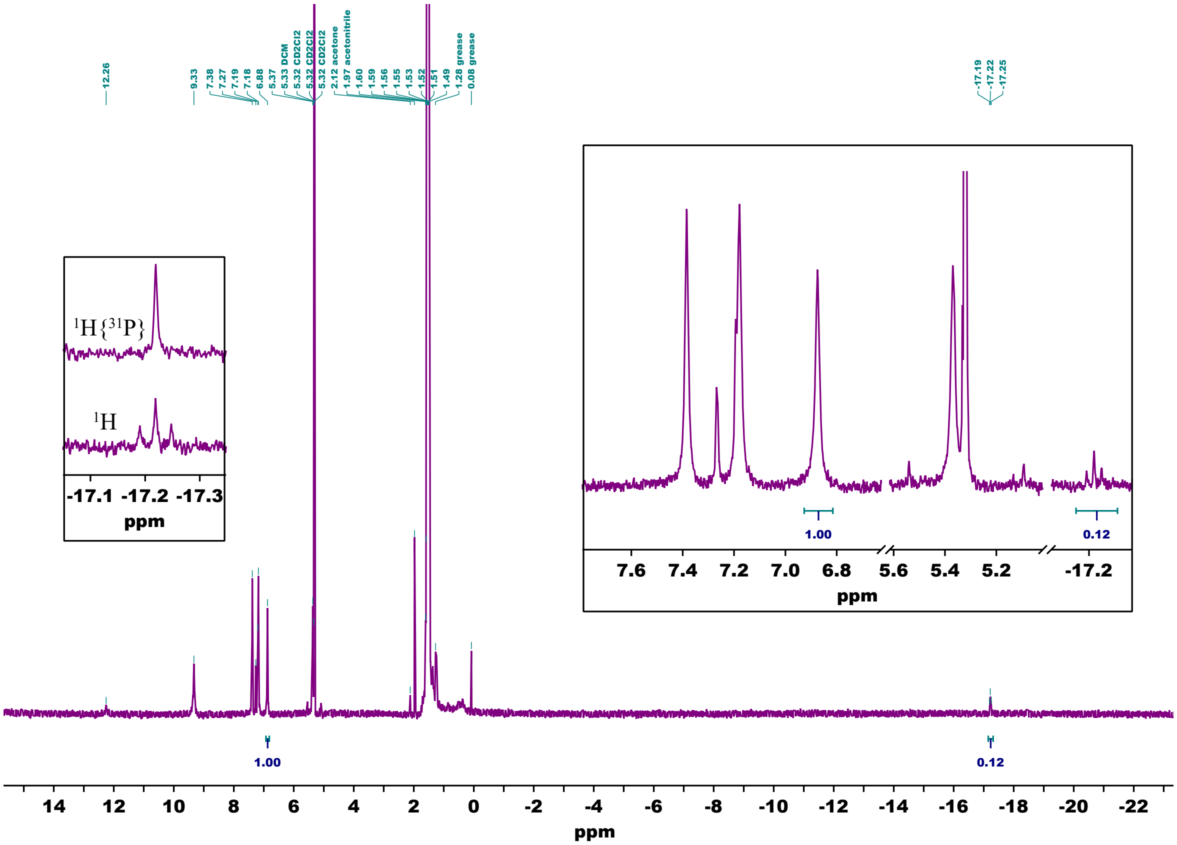

Figure S14. ^{1}H NMR (400 MHz, DCM-d_2) spectrum of a solution of **[$^{\mathbf{LH}}$Ir][Br]** collected after heating. (Left Inset) Ir–H resonance in the ^{1}H and ^{1}H{^{31}P} NMR spectrum.

Synthesis and Characterization of [$^{\text{LH}}$Ir][I]

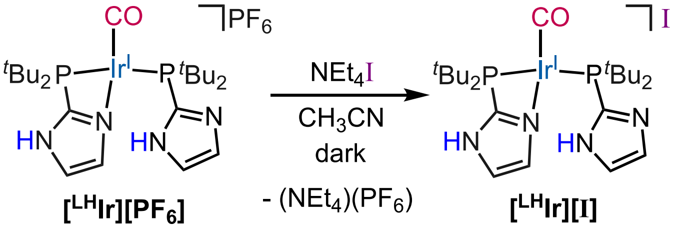

In the dark, NEt$_4$I (60.0 mg, 0.233 mmol) and **[$^{\text{LH}}$Ir][PF$_6$]** (182 mg, 0.231 mmol) were weighed in two separate vials (the reactions were carried out in the dark to avoid any potential decomposition of the iodide anion). 4 mL of acetonitrile (enough to dissolve) was added to both vials, and the solution of NEt$_4$I was transferred to the solution of **[$^{\text{LH}}$Ir][PF$_6$]** and stirred vigorously. The product **[$^{\text{LH}}$Ir][I]** started precipitating out of solution within few minutes, and at this point the stirring was stopped and the precipitate was allowed to settle for 5 minutes. The yellow precipitate was then isolated by filtering the solution through a medium porosity glass fitted funnel, washing with 5 mL acetonitrile, and drying under vacuum. Single crystals suitable for X-ray diffraction were grown by preparing a saturated acetonitrile solution of the product **[$^{\text{LH}}$Ir][I]** at room temperature, and then storing it at -30 °C overnight.

Yield: 155 mg (87%).

Note: The product can be washed with more acetonitrile at the expense of some of the yield if NMR spectral signals for (NEt$_4$)(PF$_6$) are present. The product was stable to ambient light.

^{1}H NMR (400 MHz, DCM-d_2): δ 14.31 (br, 1H), 9.23 (br, 1H), 7.39 (s, 1H), 7.19 (s, 1H), 6.93 (s, 1H), 5.35 (s, 1H), 1.53 (two overlapping d, 36H).

^{31}P{^{1}H} NMR (162 MHz, DCM-d_2): δ 50.07 (d, $^2J_{\text{P–P}}$ = 253 Hz), 39.72 (d, $^2J_{\text{P–P}}$ = 253 Hz).

^{13}C{^{1}H} NMR (126 MHz, DCM-d_2): δ 176.63 (t, $^2J_{\text{P–C}}$ = 10 Hz), 152.04 (d, $^1J_{\text{P–C}}$ = 37 Hz), 139.61 (d, $^1J_{\text{P–C}}$ = 59 Hz), 131.40 (d, $^3J_{\text{P–C}}$ = 8 Hz), 127.30 (d, $^3J_{\text{P–C}}$ = 11 Hz), 120.29 (s), 119.15 (s), 38.67 (d, $^1J_{\text{P–C}}$ = 25 Hz), 35.91 (d, $^1J_{\text{P–C}}$ = 18 Hz), 30.25 (s), 30.21 (s).

IR (ν_{co}, DCM-d_2): 1970 cm^{-1}

Accurate Mass Measurement (ESI+, TOF) $C_{23}H_{43}IrN_4OP_2$: Theoretical Mass = 645.2466, Observed Mass = 645.2464.

Anal. Calcd. For **[$^{\text{LH}}$Ir][I]**, $C_{23}H_{42}IIrN_4OP_2$: C, 35.80; H, 5.49; N, 7.26. Found: C, 35.52; H, 5.25; N, 7.16.

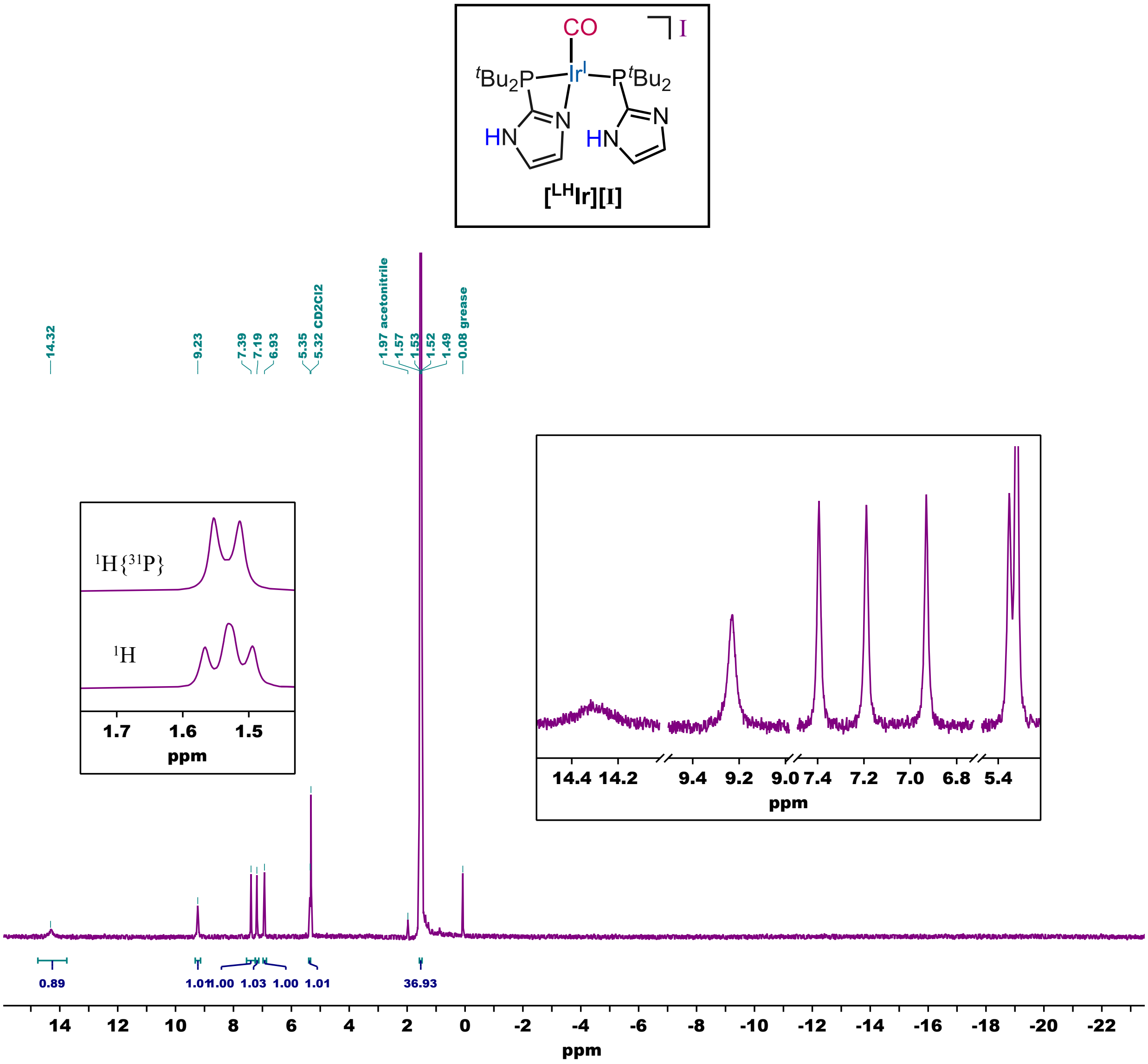

Figure S15. ^1H NMR (400 MHz, DCM-d_2) spectrum of **[^{LH}Ir][I]**. (Left Inset) Aliphatic region of the ^1H and $^1H\{^{31}P\}$ NMR spectrum.

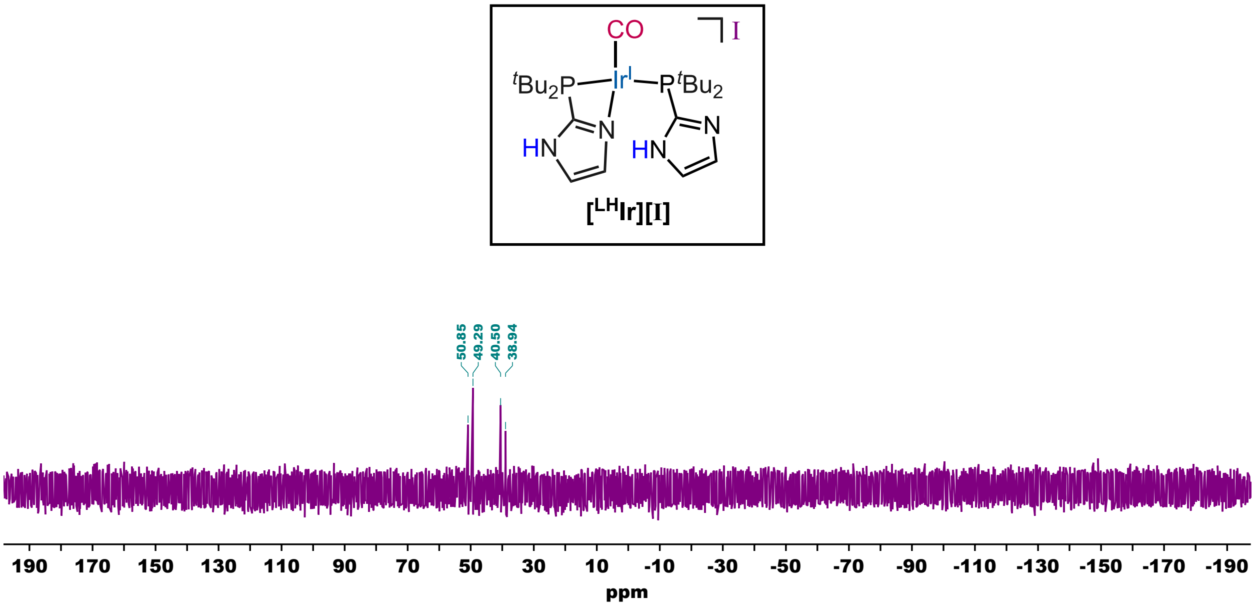

Figure S16. ^{31}P{^{1}H} NMR (162 MHz, DCM-d_2) spectrum of **[^{LH}Ir][I]**.

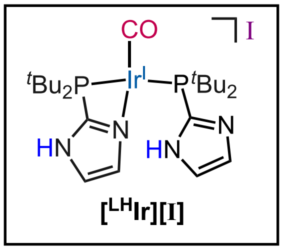

[^{LH}Ir][I]

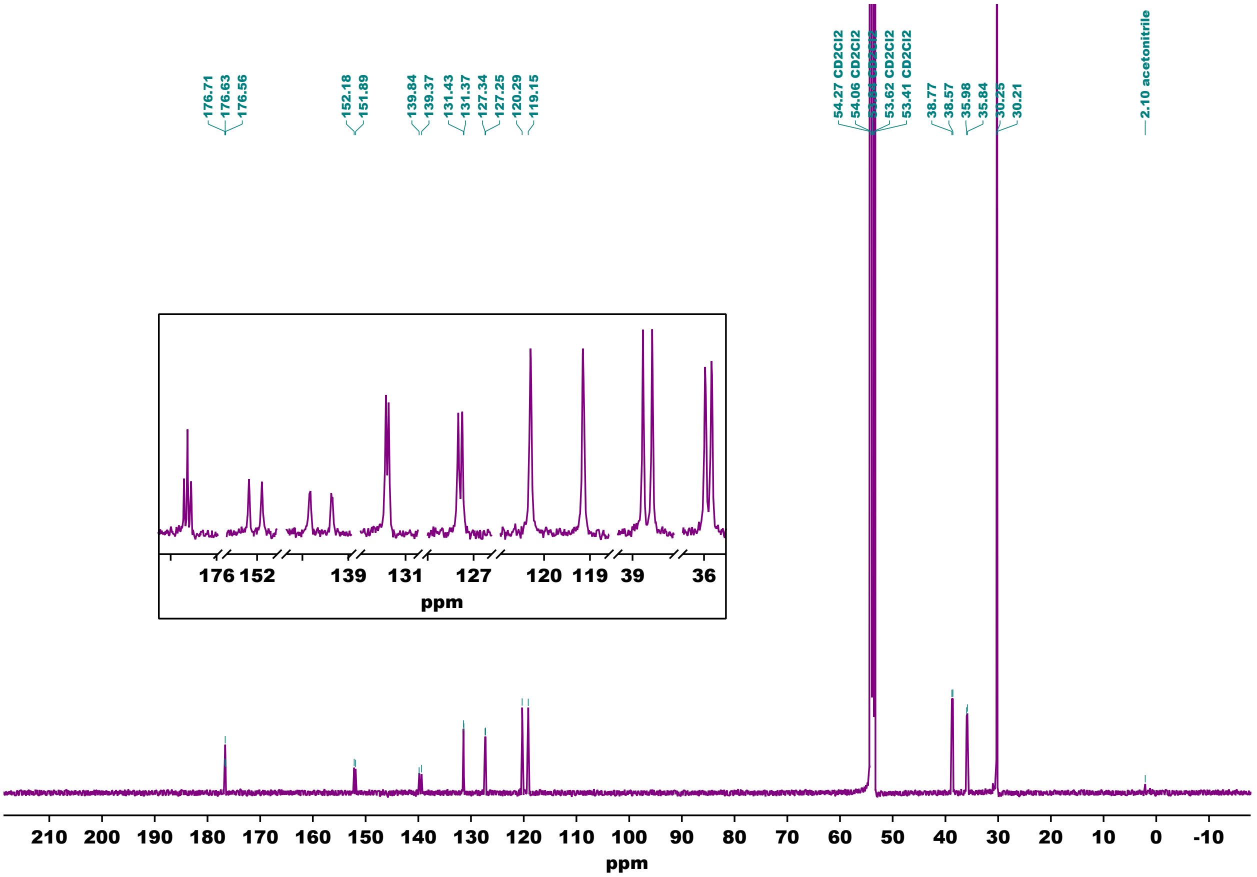

Figure S17. $^{13}C\{^1H\}$ NMR (126 MHz, DCM-d_2) spectrum of **[^{LH}Ir][I]**.

Heating a DCM-d_2 solution of [$^{\mathbf{LH}}$Ir][I]

2.10 mg (3.13×10^{-3} mmol) of **[$^{\mathbf{LH}}$Ir][I]** was dissolved in 0.40 mL DCM-d_2 inside a glovebox. The solution was transferred to a J. Young NMR tube and then heated at 60 °C for 2 days. The calculated K_{eq} value is provided below on page S52.

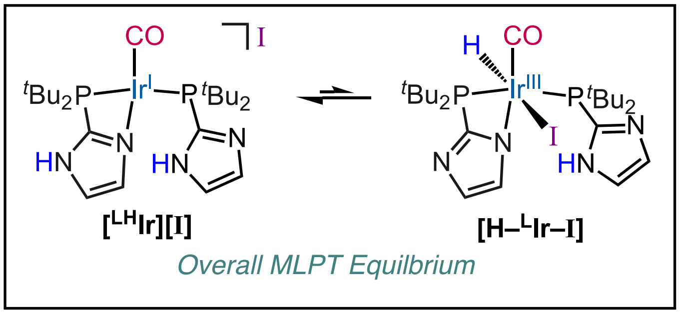

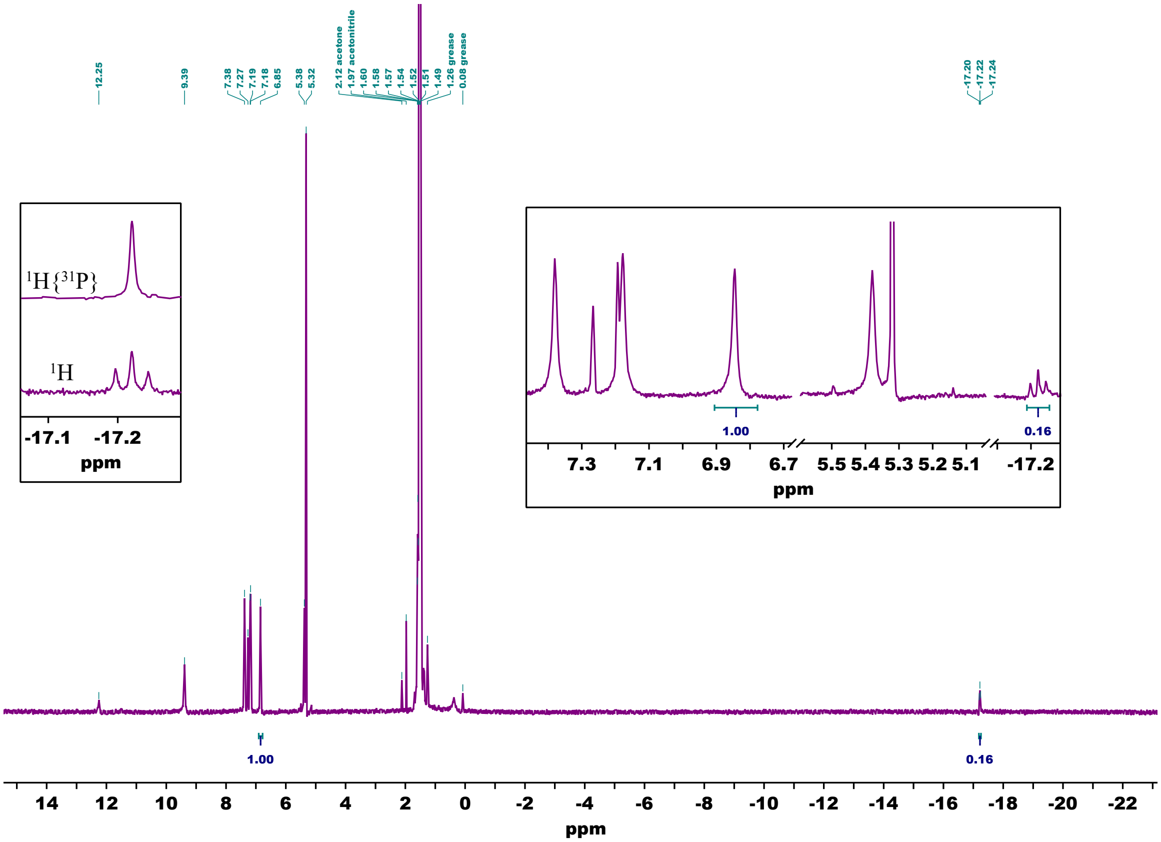

Figure S18. ^{1}H NMR (400 MHz, DCM-d_2) spectrum of a solution of **[$^{\mathbf{LH}}$Ir][Br]** collected after heating. (Left Inset) Ir–H resonance in the ^{1}H and ^{1}H{^{31}P} NMR spectrum.

Synthesis and Characterization of [$^{\mathbf{LH}}$Ir][F]

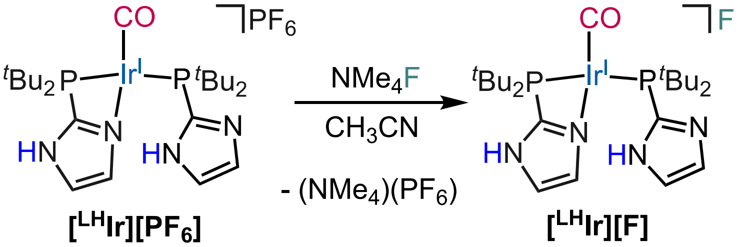

[$^{\mathbf{LH}}$Ir][PF$_6$] (215 mg, 0.271 mmol) and NMe_4F (25.7 mg, 0.276 mmol) were weighed in two separate vials. 3 mL of acetonitrile was added to both vials, and the solution of **[$^{\mathbf{LH}}$Ir][PF$_6$]** was transferred to the suspension of NMe_4F. Upon stirring for few minutes, the solution turned homogenous. Upon further stirring (total 10 minutes), the solution turned hazy and stirring was stopped. The reaction mixture was then stored at -30 °C for 5 hours (or overnight) and the product **[$^{\mathbf{LH}}$Ir][F]** precipitated out. The yellow precipitate was isolated by filtering the solution through a medium porosity glass fritted funnel, washing with 3 mL acetonitrile, and drying under vacuum. Single crystals suitable for X-ray diffraction were grown by preparing a saturated acetonitrile solution of the product **[$^{\mathbf{LH}}$Ir][F]** at room temperature, and then storing it at -30 °C overnight.
Yield: 151 mg (84%).
Note: The product can be washed with more acetonitrile at the expense of some of the yield if NMR spectral signals for $(NMe_4)(PF_6)$ are present. NMe_4F must be handled in dry atmospheres, ideally in an inert gas filled glovebox, because of its instability to moisture.

As described in the main text, when solid **[$^{\mathbf{LH}}$Ir][F]** was dissolved in DCM-*d*$_2$, the NMR spectral signals observed were more consistent with its description as a hydrogen bonded adduct **[$^{\mathbf{LH}}$Ir•F]**:

^{1}H NMR (400 MHz, DCM-*d*$_2$): δ 16.15 (br, 1H), 9.34 (br, 1H), 7.37 (s, 1H), 7.14 (s, 1H), 6.71 (s, 1H), 5.44 (s, 1H), 1.49 (two overlapping d, 36H).

^{31}P{^{1}H} NMR (162 MHz, DCM-*d*$_2$): δ 50.02 (d, $^2J_{P–P}$ = 254 Hz), 36.20 (d, $^2J_{P–P}$ = 256 Hz).

^{19}F{^{1}H} NMR (376 MHz, DCM-*d*$_2$): δ -150.01 (br)

^{13}C{^{1}H} NMR (126 MHz, DCM-*d*$_2$): δ 176.93 (t, $^2J_{P–C}$ could not be resolved), 152.28 (d, $^1J_{P–C}$ = 53 Hz), 140.28 (d, $^1J_{P–C}$ = 59 Hz), 131.15 (d, $^3J_{P–C}$ = 8 Hz), 127.28 (d, $^3J_{P–C}$ = 11 Hz), 125.19 (s), 118.80 (s), 38.40 (d, $^1J_{P–C}$ = 25 Hz), 35.59 (d, $^1J_{P–C}$ = 20 Hz), 30.21 (d, $^2J_{P–C}$ = 5 Hz), 30.00 (d, $^2J_{P–C}$ = 5 Hz).

IR (ν_{co}, DCM-d_2): 1952 cm^{-1}

Accurate Mass Measurement (ESI+, TOF) $C_{23}H_{42}IrN_4OP_2$: Theoretical Mass = 645.2463, Observed Mass = 645.2485.

Anal. Calcd. For **[^{LH}Ir][F]** (+ H_2O), $C_{23}H_{44}FIrN_4O_2P_2$: C, 40.52; H, 6.51; N, 8.22. Found: C, 40.07; H, 6.15; N, 8.77.

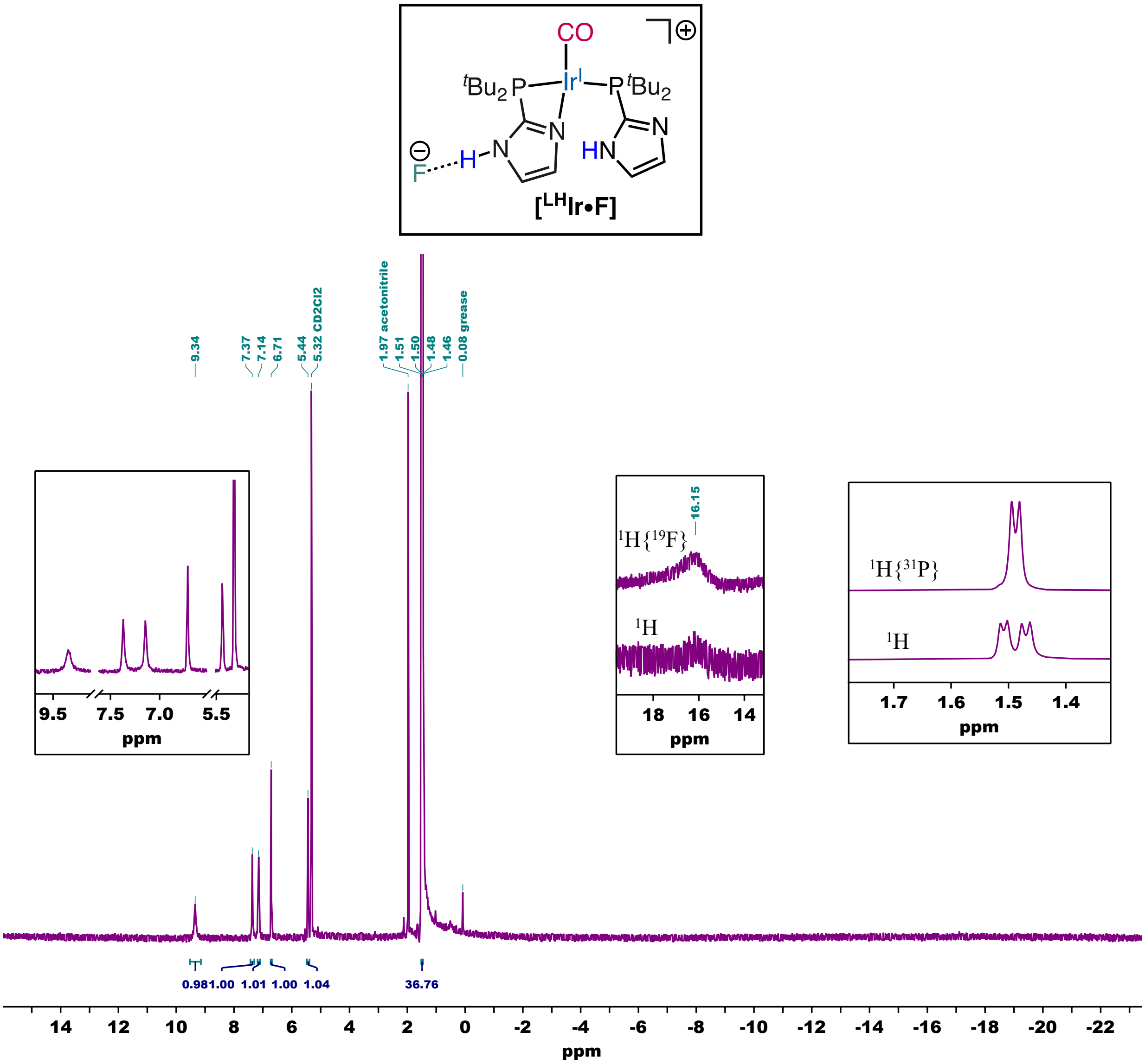

Figure S19. ^{1}H NMR (400 MHz, DCM-d_2) spectrum of **[$^{\text{LH}}$Ir•F]**. (Middle Inset) Downfield region of the ^{1}H and ^{1}H{^{19}F} NMR spectrum showing a broad resonance for the N–H proton involved in hydrogen bonding with the fluoride anion. (Right Inset) Aliphatic region of the ^{1}H and ^{1}H{^{31}P} NMR spectrum.

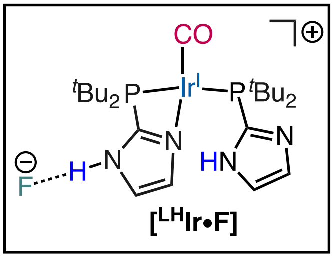

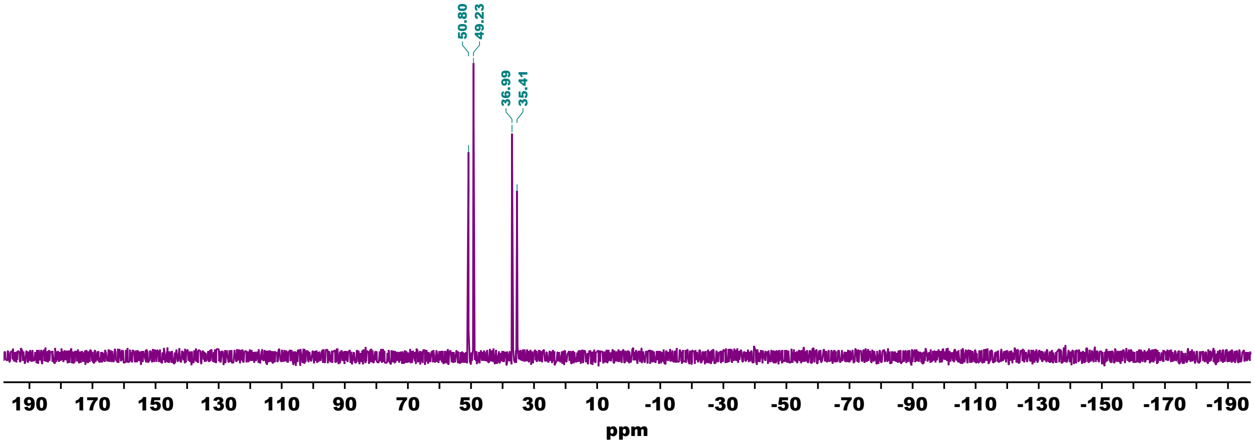

Figure S20. ^{31}P{^{1}H} NMR (162 MHz, DCM-d_2) spectrum of **[^{LH}Ir•F]**.

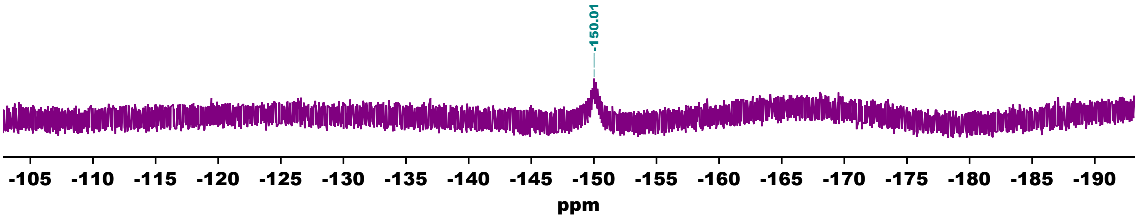

Figure S21. ^{19}F{^{1}H} NMR (376 MHz, DCM-d_2) spectrum of **[^{LH}Ir•F]**.

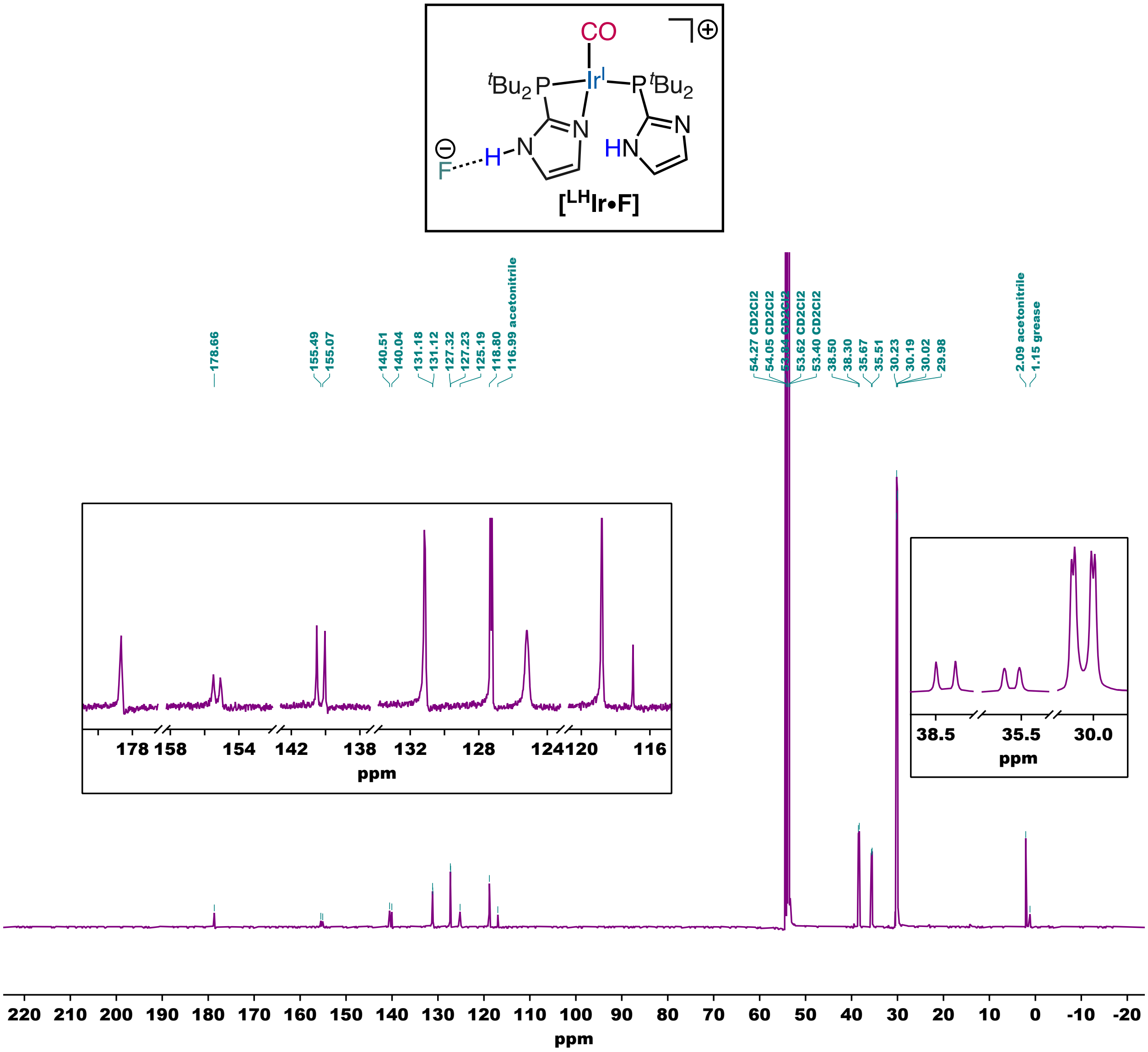

Figure S22. $^{13}C\{^{1}H\}$ NMR (126 MHz, DCM-d_2) spectrum of **[^{LH}Ir•F]**.

Synthesis and Characterization of [^{L}Ir]

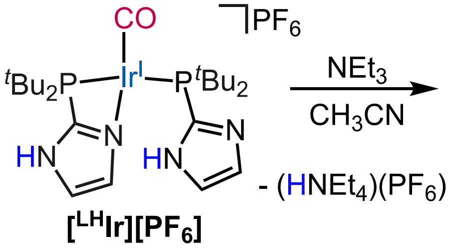

(This synthesis can be performed in air) To a 10 mL acetonitrile solution of **[^{LH}Ir][PF$_6$]** (90.0 mg, 0.114 mmol), NEt$_3$ (0.11 mL, 0.79 mmol) was added using a syringe. After stirring for one minute, the solvent was removed under vacuum. Approximately 20 mL of diethyl ether was added to the dried reaction mixture, and the resulting suspension was filtered through celite. Evaporation of the filtrate afforded a yellow powder of the product **[^{L}Ir].** Single crystals suitable for X-ray diffraction were grown by preparing a saturated acetonitrile solution of the product **[^{L}Ir]** at room temperature, and then storing it at -30 °C overnight.

Yield: 38 mg (52%).

^{1}H NMR (400 MHz, DCM-d_2): δ 9.38 (br, 1H), 7.36 (s, 1H), 7.11 (s, 1H), 6.64 (s, 1H), 5.58 (d, 1H, $^{4}J_{P\text{–}H}$ = 4 Hz), 1.47 (two overlapping d, 36H).

^{31}P{^{1}H} NMR (162 MHz, DCM-d_2): δ 50.29 (d, $^{2}J_{P\text{–}P}$ = 259 Hz), 35.68 (d, $^{2}J_{P\text{–}P}$ = 259 Hz).

^{13}C NMR (126 MHz, DCM-d_2): δ 180.23 (t, $^{2}J_{P\text{–}C}$ = 9 Hz), 157.88 (d, $^{1}J_{P\text{–}C}$ = 67 Hz), 140.96 (dd, $^{1}J_{P\text{–}C}$ = 60 Hz, $^{2}J_{C\text{–}C}$ = 4 Hz), 131.16 (d, $^{3}J_{P\text{–}C}$ = 8 Hz), 128.69 (d, $^{3}J_{P\text{–}C}$ = 10 Hz), 127.47 (d, $^{3}J_{P\text{–}C}$ = 11 Hz), 118.26 (s), 38.20 (d, $^{1}J_{P\text{–}C}$ = 25 Hz), 35.28 (dd, $^{1}J_{P\text{–}C}$ = 21 Hz, $^{2}J_{C\text{–}C}$ = 4 Hz), 30.18 (m).

IR (ν_{co}, DCM-d_2): 1947 cm^{-1}

Accurate Mass Measurement (ESI+, TOF) $C_{23}H_{41}IrN_4OP_2$: Theoretical Mass (M+H) = 645.2463, Observed Mass = 645.2451.

Anal. Calcd. For **[^{L}Ir]**, $IrP_2N_4C_{23}OH_{41}$: C, 42.91; H, 6.42; N, 8.70. Found: C, 42.69; H, 6.43; N, 8.96.

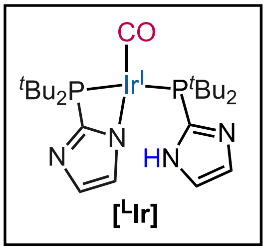

[^{L}Ir]

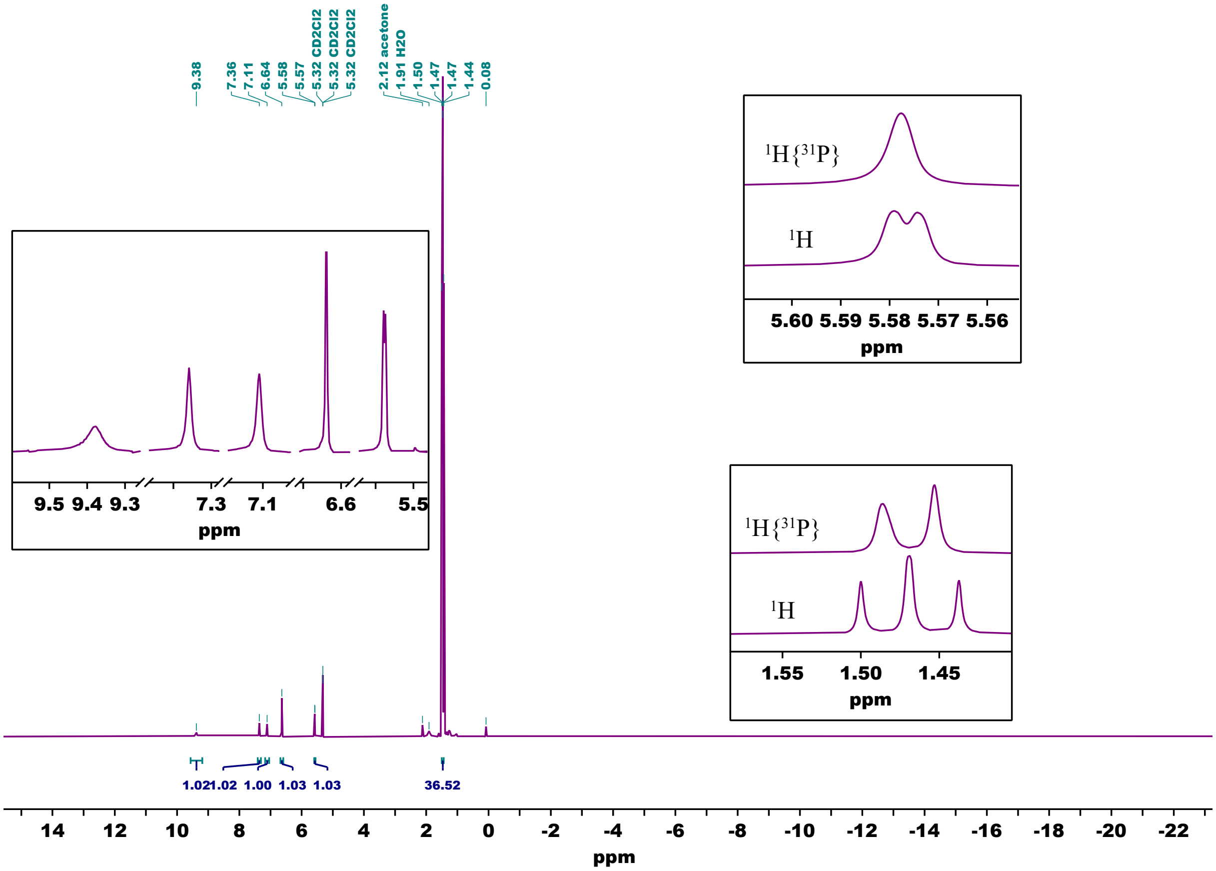

Figure S23. ^{1}H NMR (500 MHz, DCM-d_2) spectrum of **[^{L}Ir]**. (Right Inset) Selected aromatic and aliphatic region of the ^{1}H and ^{1}H{^{31}P} NMR spectrum.

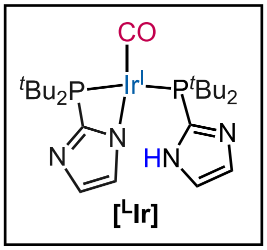

Figure S24. $^{31}P\{^1H\}$ NMR (162 MHz, DCM-d_2) spectrum of **[^{L}Ir]**.

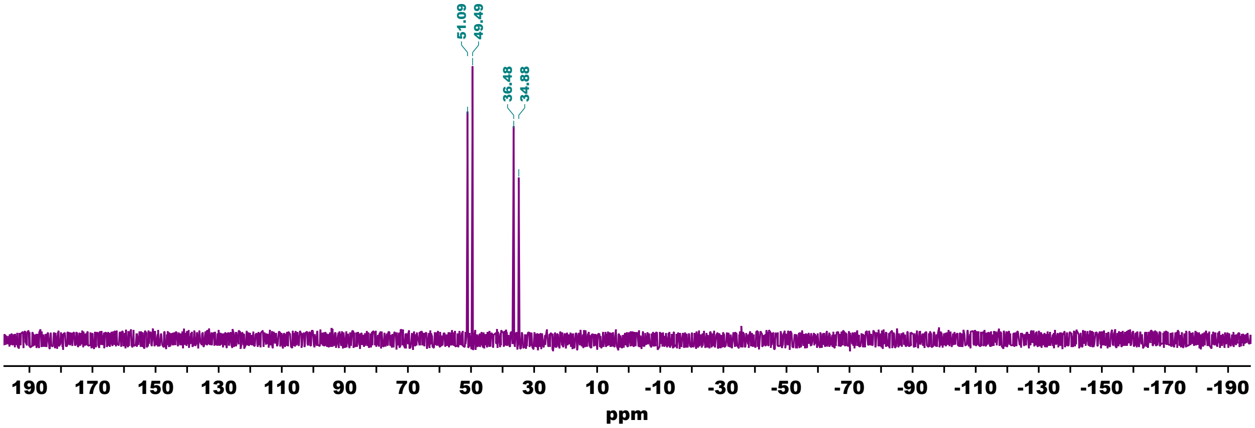

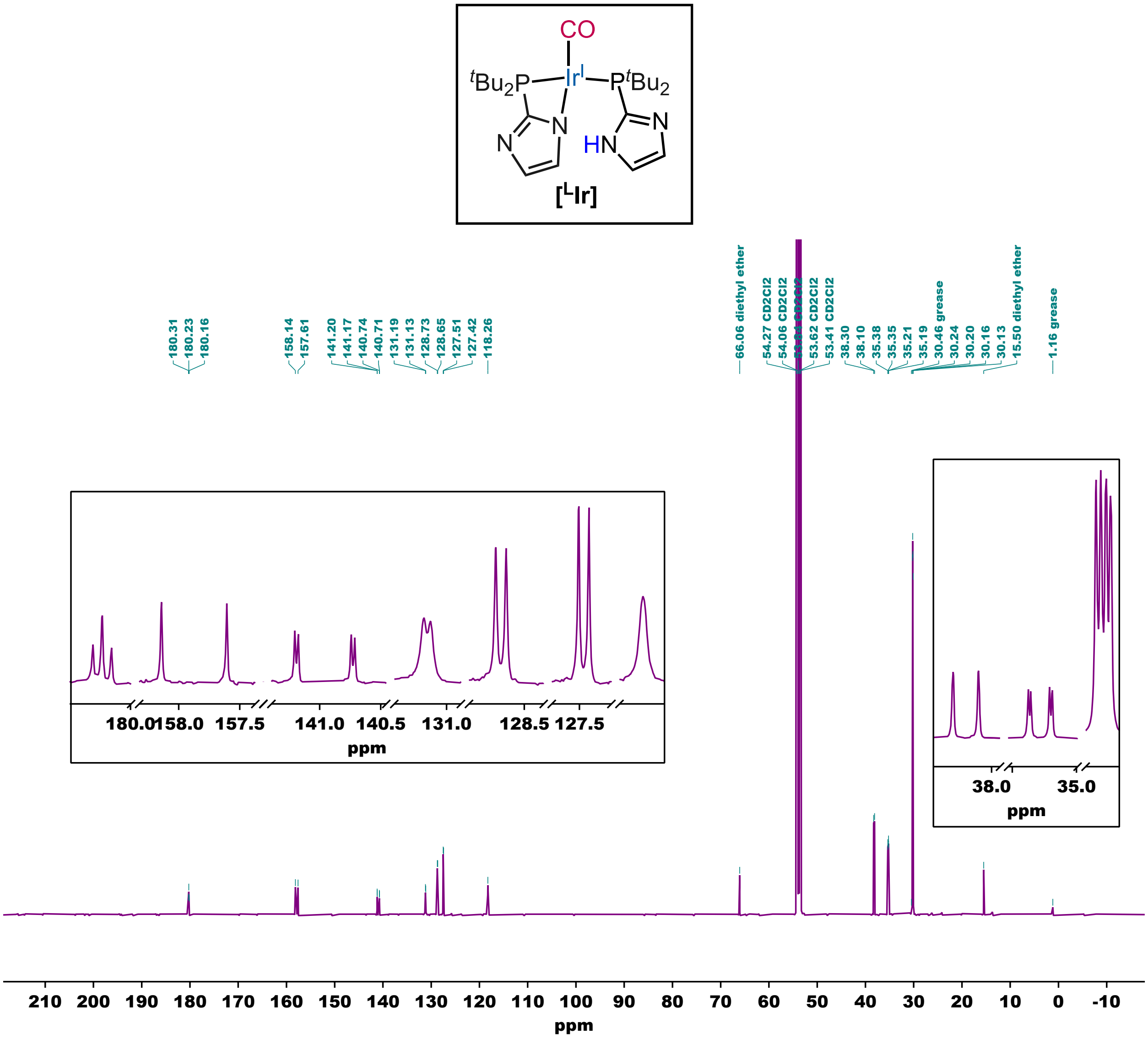

Figure S25. $^{13}C\{^1H\}$ NMR (126 MHz, DCM-d_2) spectrum of **[^{L}Ir]**.

Probing the Equilibria

Addition of excess Cl anion to the DCM-d_2 solution of [^{LH}Ir][Cl]: *(in situ)* generation of [^{LH}Ir–Cl]

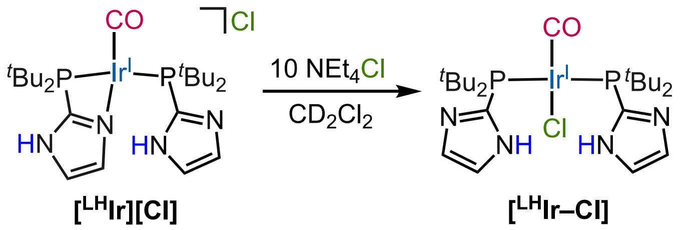

[^{LH}Ir][Cl] (4.1 mg, 0.0060 mmol) and NBu_4Cl (22.1 mg, 0.060 mmol) were weighed in two separate vials inside a glovebox. 0.45 mL DCM-d_2 was added to the vial containing NBu_4Cl and this solution was transferred to the vial containing **[^{LH}Ir][Cl]**. After thorough mixing using a pipette, the resulting solution was transferred to a J. Young tube to which 0.05 mL of 1,3,5-trimethoxybenzene's 4.6 mg/mL standard solution (0.23 mg, 0.0014 mmol) was also added (internal standard). In the ^{1}H NMR spectrum (Figure S26), 2 new resonances in the aromatic region (for the two sets of equivalent protons on the imidazoles) were observed. Additionally, a singlet in the ^{31}P{^{1}H} NMR spectrum (Figure S27) was observed. These data are consistent with the generation of **[^{LH}Ir–Cl]** in solution. No signals for either **[^{LH}Ir][Cl]** or **[H–^{L}Ir–Cl]** were present after addition of excess Cl anion to **[^{LH}Ir][Cl]**. Spectroscopic Yield: > 99%.

Spectroscopic data for the in situ generated **[^{LH}Ir–Cl]**:

^{1}H NMR (400 MHz, DCM-d_2): δ 13.46 (br, 2H), 7.22 (s, 2H), 7.02 (s, 2H), 1.52 (br, 36H).

^{31}P{^{1}H} NMR (162 MHz, DCM-d_2): δ 33.06 (br)

ν_{co} (DCM-d_2): 1956 cm^{-1}

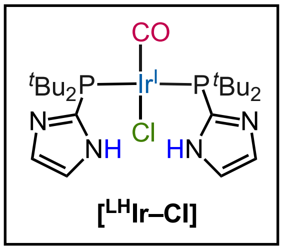

[^{LH}Ir–Cl]

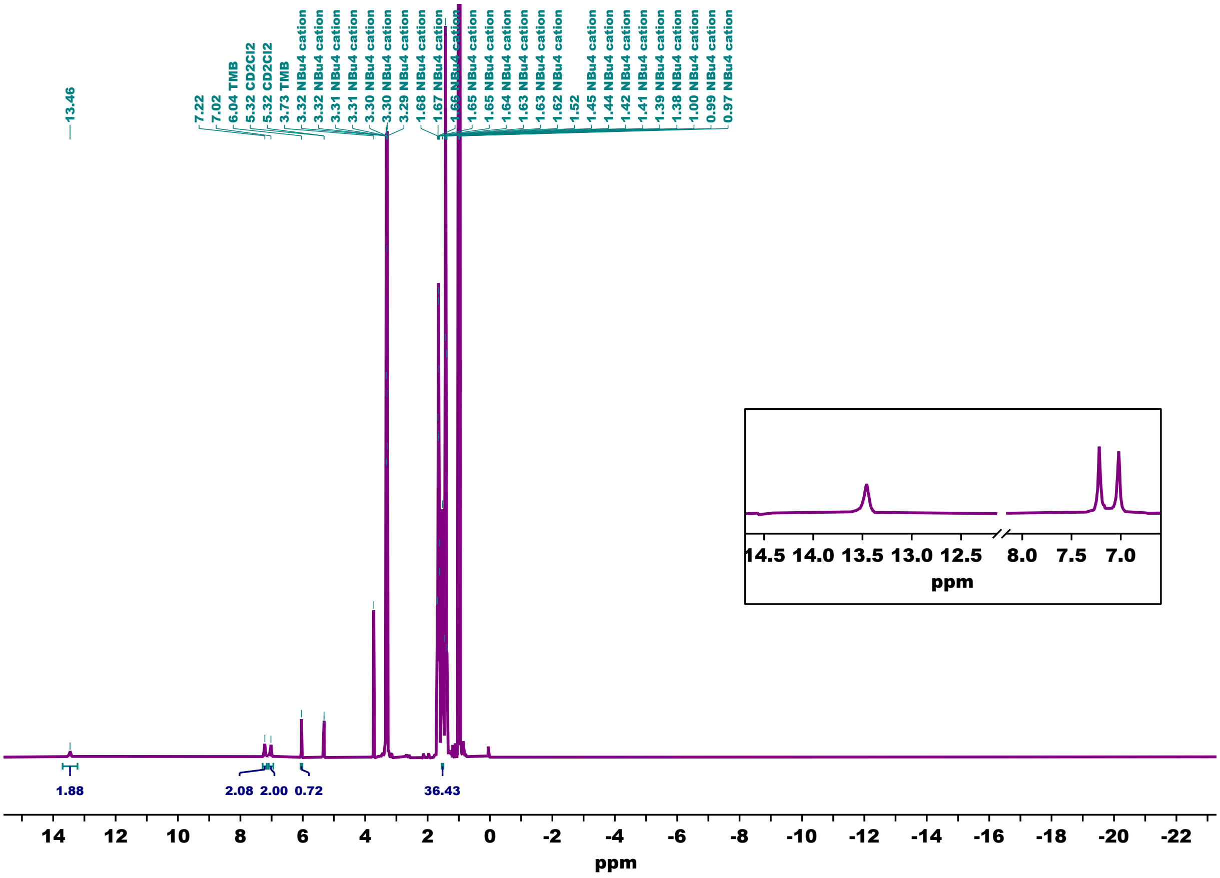

Figure S26. ^{1}H NMR (500 MHz, DCM-d_2) spectrum of the *in situ* generated **[^{LH}Ir–Cl]**.

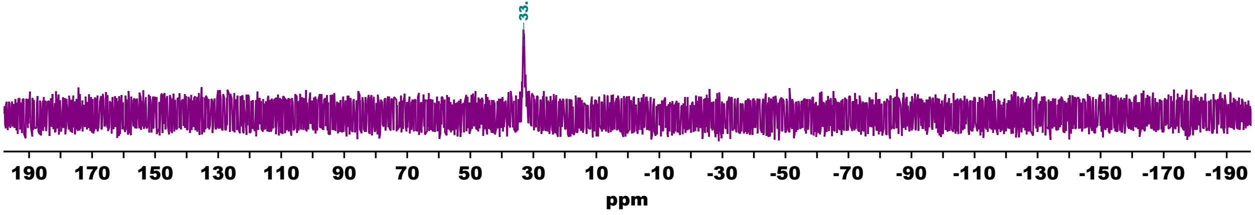

Figure S27. ^{31}P{^{1}H} NMR (162 MHz, DCM-d_2) spectrum of the *in situ* generated **[^{LH}Ir–Cl]**.

Addition of excess $(NBu_4)(PF_6)$ salt to the *in situ* generated **[^{LH}Ir–Cl]** in DCM-d_2

To evaluate if ionic strength of the solution impacted the MLPT equilibrium, a DCM-d_2 solution of the *in situ* generated **[^{LH}Ir–Cl]** was titrated with $(NBu_4)(PF_6)$ salt. The solids **[^{LH}Ir][Cl]** (3.40 mg, 0.005 mmol) and NEt_4Cl (8.30 mg, 0.050 mmol) were weighed in two separate vials inside a glovebox. 0.48 mL DCM-d_2 was added to the vial containing NEt_4Cl and this solution was transferred to the vial containing **[^{LH}Ir][Cl]**. After thorough mixing using a pipette, the resulting solution of **[^{LH}Ir–Cl]** was transferred to a J. Young tube for analysis *via* ^{1}H NMR spectroscopy. Thereafter, a total of 10 molar equivalents of $(NBu_4)(PF_6)$ salt was added to the solution of the *in situ* generated **[^{LH}Ir–Cl]** portion-wise (^{1}H NMR was collected after cumulative additions of 2, 5, and 10 molar equivalents; Figure S28). It can be noted that a profound increase in the ionic strength of the solution by addition of excess ionic salt has almost no impact on the signals; the N–H peak, for example, shifts downfield by a mere 0.03 ppm.

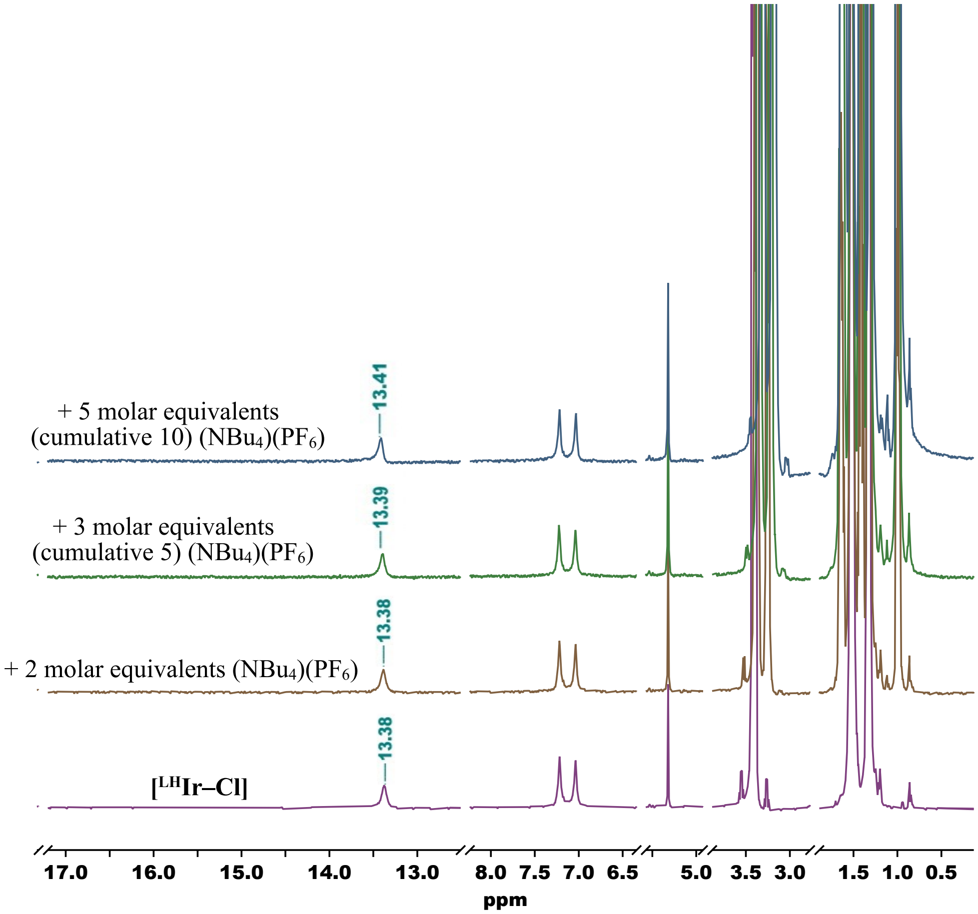

Figure S28. Stacked ^{1}H NMR (500 MHz, DCM-d_2) spectra of the titration of the *in situ* generated **[$^{\mathbf{LH}}$Ir–Cl]** with $(NBu_4)(PF_6)$.

Addition of excess Br anion to the DCM-d_2 solution of [$^{\text{LH}}$Ir][Br]: *(in situ)* generation of [$^{\text{LH}}$Ir–Br] upon heating

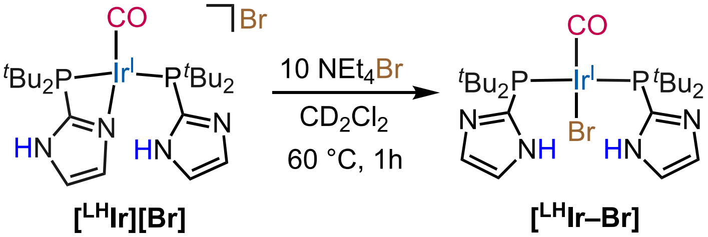

[$^{\text{LH}}$Ir][Br] (4.4 mg, 0.0060 mmol) and NBu_4Br (19.7 mg, 0.061 mmol) were weighed in two separate vials inside a glovebox. DCM-d_2 (0.38 mL) was added to the vial containing NBu_4Br and this solution was transferred to the vial containing **[$^{\text{LH}}$Ir][Br]**. After thorough mixing using a pipette, the resulting solution was transferred to a J. Young tube to which 0.12 mL of 1,3,5-trimethoxybenzene's 4.6 mg/mL standard solution (0.55 mg, 0.0033 mmol) was also added (internal standard). The reaction mixture was heated at 60 °C for an hour, following which the spectroscopical analysis was carried out. In the ^{1}H NMR spectrum (Figure S29), 2 new resonances in the aromatic region (for the two sets of equivalent protons on the imidazoles) were observed. Additionally, a singlet in the ^{31}P{^{1}H} NMR spectrum (Figure S30) was observed. These data are consistent with the generation of **[$^{\text{LH}}$Ir–Br]** in solution. No signals for either **[$^{\text{LH}}$Ir][Br]** or **[H–$^{\text{L}}$Ir–Br]** were present after addition of excess Br anion to **[$^{\text{LH}}$Ir][Br]**. Spectroscopic Yield ~ 97%.

Spectroscopic data for the in situ generated **[$^{\text{LH}}$Ir–Br]**:

^{1}H NMR (500 MHz, DCM-d_2): δ 13.01 (br, 2H), 7.23 (s, 2H), 7.03 (s, 2H), 1.52 (br, 36H).

^{31}P{^{1}H} NMR (202 MHz, DCM-d_2): δ 32.90 (br)

ν_{co} (DCM-d_2): 1962 cm^{-1}

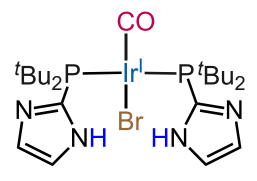

[^{LH}Ir–Br]

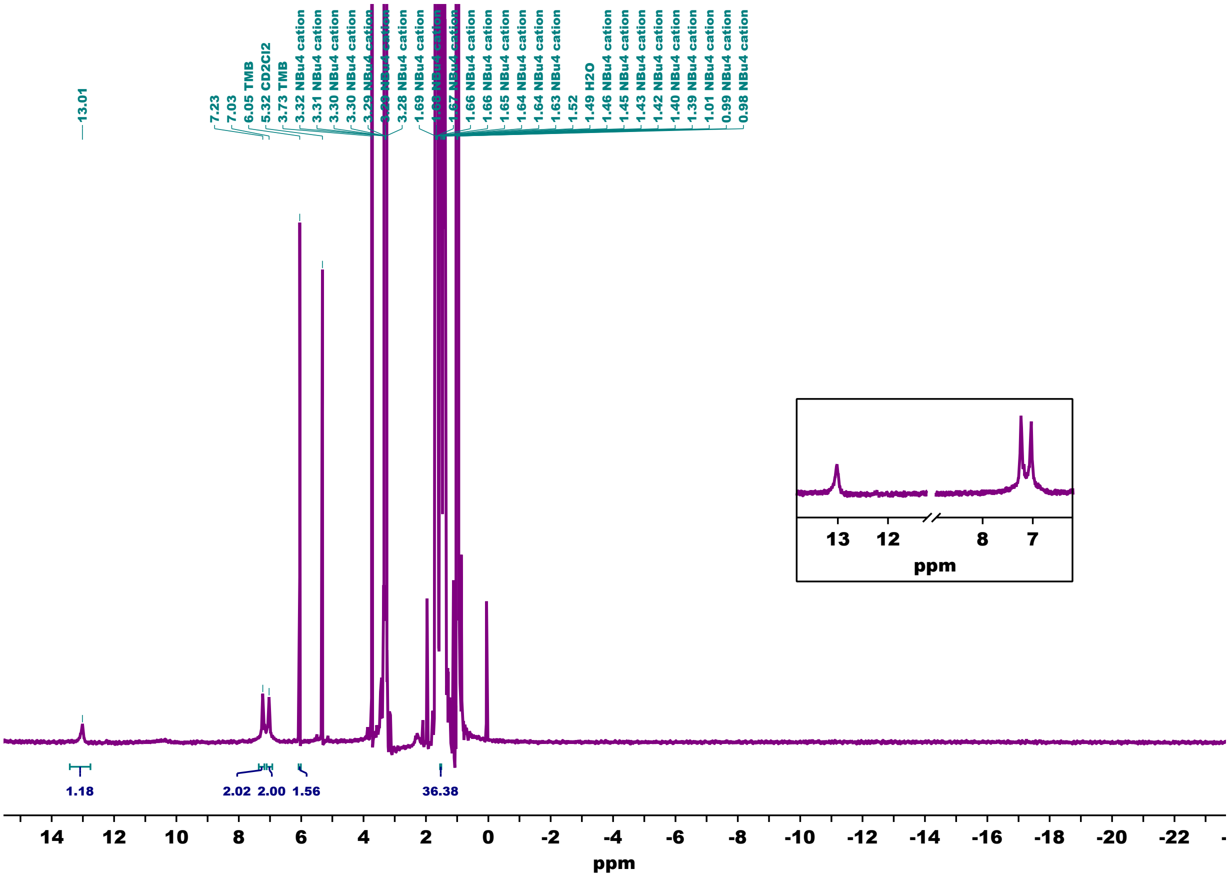

Figure S29. ^{1}H NMR (500 MHz, DCM-d_2) spectrum of the *in situ* generated **[^{LH}Ir–Br]**.

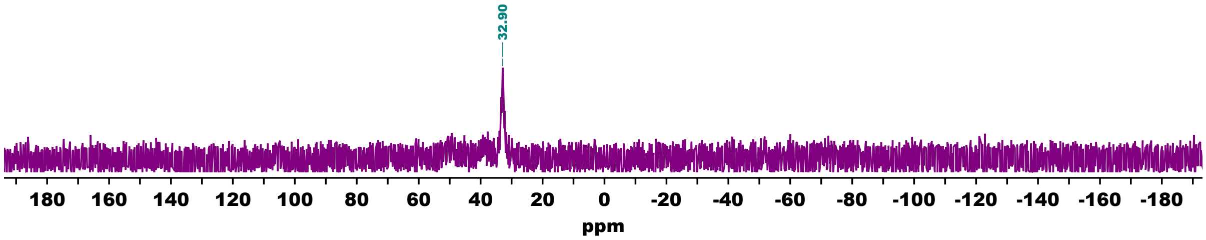

Figure S30. ^{31}P{^{1}H} NMR (202 MHz, DCM-d_2) spectrum of the *in situ* generated **[^{LH}Ir–Br]**.

Addition of excess I anion to the DCM-d_2 solution of [^{LH}Ir][I]: *(in situ)* generation of (90% [^{LH}Ir–I] + 10% [H–^{L}Ir–I]) upon heating

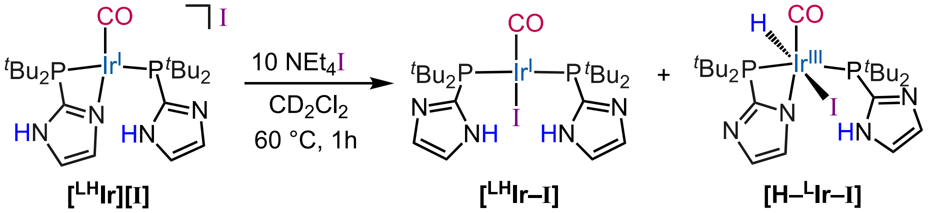

[^{LH}Ir][I] (4.6 mg, 0.0060 mmol) and NBu$_4$I (22.1 mg, 0.060 mmol) were weighed in two separate vials inside a glovebox in the dark. DCM-d_2 (0.38 mL) was added to the vial containing NBu$_4$I and this solution was transferred to the vial containing **[^{LH}Ir][I]**. After thorough mixing using a pipette, the resulting solution was transferred to a J. Young tube to which 0.12 mL of 1,3,5-trimethoxybenzene's 4.6 mg/mL standard solution (0.55 mg, 0.0033 mmol) was also added (internal standard). The reaction mixture was heated at 60 °C for an hour, following which the spectroscopical analysis was carried out. Just like the bromide and chloride examples described above, two singlets in the aromatic region of the ^{1}H NMR spectrum (Figure S31) and a singlet in the ^{31}P{^{1}H} NMR spectrum (Figure S32) corresponding to the **[^{LH}Ir–I]** complex were again observed. However, additionally, a minor set of signals including an upfield Ir–H resonance were also observed in the ^{1}H NMR spectrum. This minor set of signals are attributed to the **[H–^{L}Ir–I]** complex. The upfield Ir–H signal was integrated relative to the peak at δ 7.00 in the ^{1}H NMR spectrum and a ratio of 0.055:1.00 was obtained, indicating that there is approximately 90% of **[^{LH}Ir–I]** species and 10% of **[H–^{L}Ir–I]** species in solution with respect to the internal standard. Spectroscopic Yield for Ir: > 99%.

Spectroscopic data for the in situ generated **[^{LH}Ir–I]:**

^{1}H NMR (500 MHz, DCM-d_2): δ 13.00 (br, 2H), 7.23 (s, 2H), 7.04 (s, 2H), 1.51 (br, 36H). *Partial signals for* **[H–^{L}Ir–I]:** δ 9.82 (br), 7.25 (s), 7.18 (s), 6.85 (shoulder), -17.25 (t).

^{31}P{^{1}H} NMR (202 MHz, DCM-d_2): δ 32.79 (br)

ν_{co} (DCM-d_2): 1962 cm^{-1}

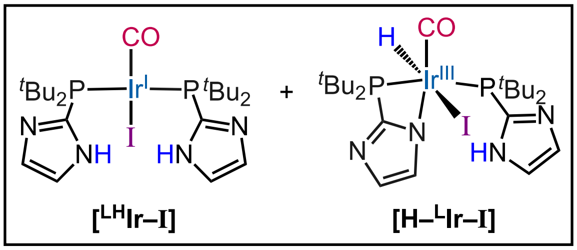

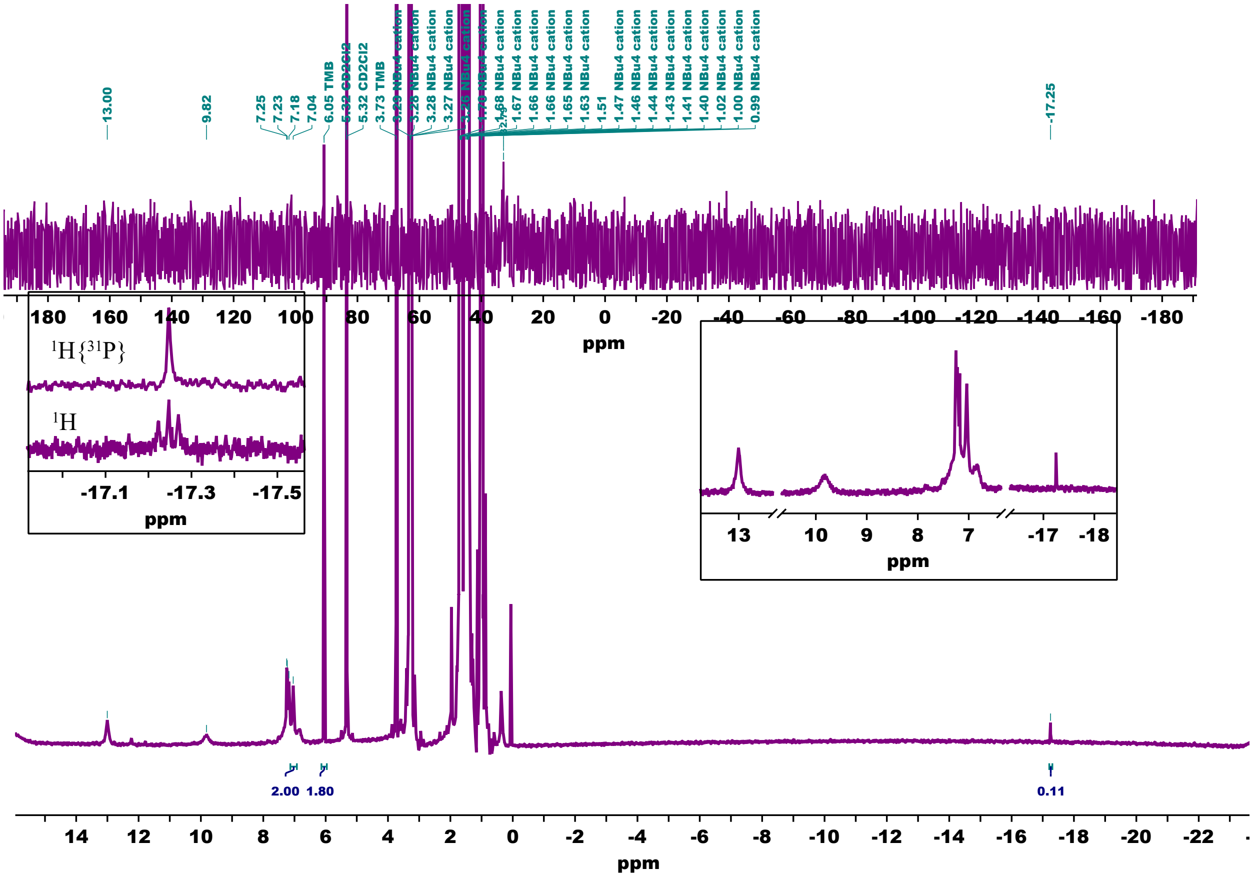

Figure S31. ^{1}H{^{31}P} NMR (500 MHz, DCM-d_2) spectrum of the *in situ* generated 94% **[^{LH}Ir–I]** + 6% **[H–^{L}Ir–I]**. (Left Inset) Ir–H resonance in the ^{1}H and ^{1}H{^{31}P} NMR spectrum.

Figure S32. ^{31}P{^{1}H} NMR (202 MHz, DCM-d_2) spectrum of the *in situ* generated **[^{LH}Ir–I]** (signals corresponding to **[H–^{L}Ir–I]** could not be resolved due to its extremely low concentration).

Addition of excess F anion to the DCM-d_2 solution of [^{LH}Ir][F]: *(in situ)* generation of [^{L}Ir]'s hydrogen bonded adduct [^{L}Ir]^{HB}

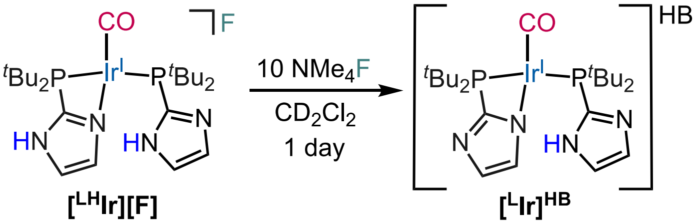

[^{LH}Ir][F] (4.0 mg, 0.0060 mmol) and NMe$_4$F (5.6 mg, 0.060 mmol) were weighed in two separate vials inside a glovebox. DCM-d_2 (0.40 mL) was added to the vial containing **[^{LH}Ir][F]** and this solution was transferred to the vial containing NMe$_4$F. After thorough mixing using a pipette, the resulting solution was transferred to a J. Young tube to which 0.10 mL of 1,3,5-trimethoxybenzene's 2.8 mg/mL standard solution (0.28 mg, 0.0017 mmol) was also added (internal standard). After letting the solution sit at room temperature for a day, spectroscopical analysis was conducted.

In the ^{1}H NMR spectrum (Figure S33), 4 separate resonances (for the two protons on each of the imidazole) were observed in the aromatic region. The most upfield aromatic resonance (δ 5.47) showed a doublet (which converted to a singlet upon P-decoupling). Such a doublet for the upfield aromatic resonance was also observed in the ^{1}H NMR spectrum of **[^{L}Ir]** (Figure S23). Other aromatic signals exhibit small $J_{H–F}$ values ranging from 1 to 2 Hz (evaluated by decoupling experiments, Figure S33), indicating the presence of a hydrogen bonded adduct of the product with excess fluoride in solution. In the $^{31}P\{^1H\}$ NMR spectrum, two sets of doublets were observed (Figure S34). Intriguingly, addition of excess F anion (NMe$_4$F) to a DCM-d_2 solution of **[^{L}Ir]** also generated the same set of NMR spectra as observed in Figures S33-35. Overall, these data suggest that addition of excess F anion to a solution **[^{LH}Ir][F]** generated the deprotonated species **[^{L}Ir]^{HB}** **(**where HB signifies a hydrogen bonded adduct). Spectroscopic Yield: > 99%.

In the ^{19}F NMR spectrum (Figure S35), signals corresponding to CD_2F_2,[5] HF_2^-,[6] and CD_2ClF[6] are observed. CD_2F_2 and CD_2ClF are formed due to the reaction of the fluoride anion with CD_2Cl_2 (with concomitant formation of stoichiometric chloride anion).[6] HF_2^- (observed by both ^{1}H and ^{19}F NMR spectroscopy) is generated likely during the deprotonation of **[^{LH}Ir][F]** to **[^{L}Ir]^{HB}**. It is noted that HF_2^- can also be formed upon the reaction of the fluoride anion with acetonitrile (trace amounts of which is present in the starting material **[$^{\mathbf{LH}}$Ir][F]**) and water (trace amounts of which might be present in CD_2Cl_2).[6]

Spectroscopic data for the in situ generated **[$^{\mathbf{L}}$Ir]$^{\mathbf{HB}}$:**

^{1}H NMR (400 MHz, DCM-d_2): δ 7.35 (d, 1H, $J_{H–F}$ = 1 Hz), 7.28 (m, 1H, $J_{H–F}$ = 1 Hz, $J_{H–P}$ couldn't be resolved), 6.63 (s, 1H), 5.46 (s, 1H, $J_{H–P}$ = 2 Hz), 1.47 (m, 36H).

^{31}P{^{1}H} NMR (162 MHz, DCM-d_2): δ 46.01 (d, $^{2}J_{P–P}$ = 259 Hz), 36.90 (d, $^{2}J_{P–P}$ = 258 Hz).

ν_{co} (DCM-d_2): 1946 cm^{-1}

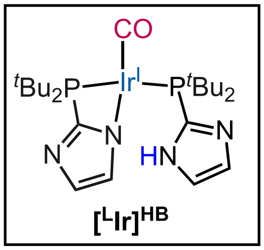

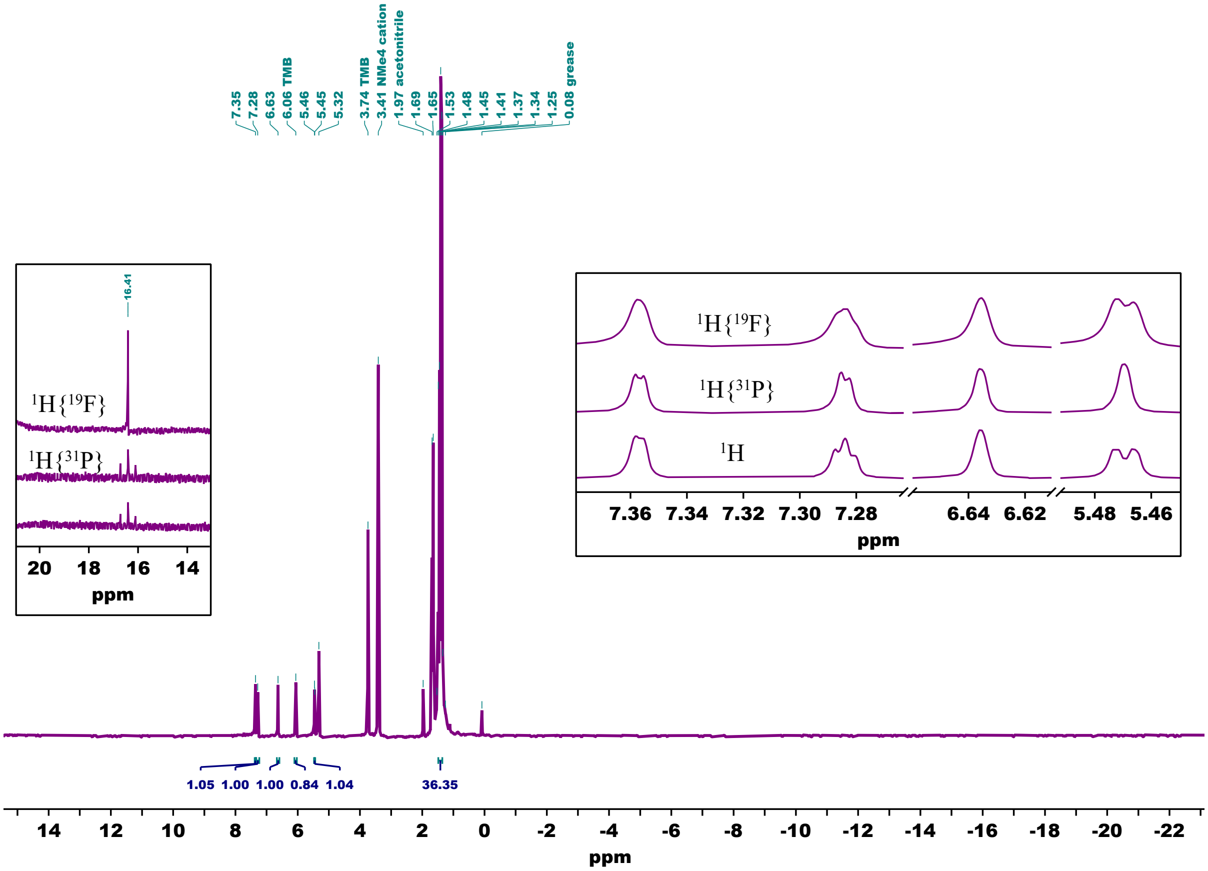

Figure S33. ^{1}H NMR (400 MHz, DCM-d_2) spectrum of the *in situ* generated **[^{L}Ir]^{HB}**. (Insets) Selected aromatic and downfield region of the ^{1}H, ^{1}H{^{31}P}, and ^{1}H{^{19}F} NMR spectrum.

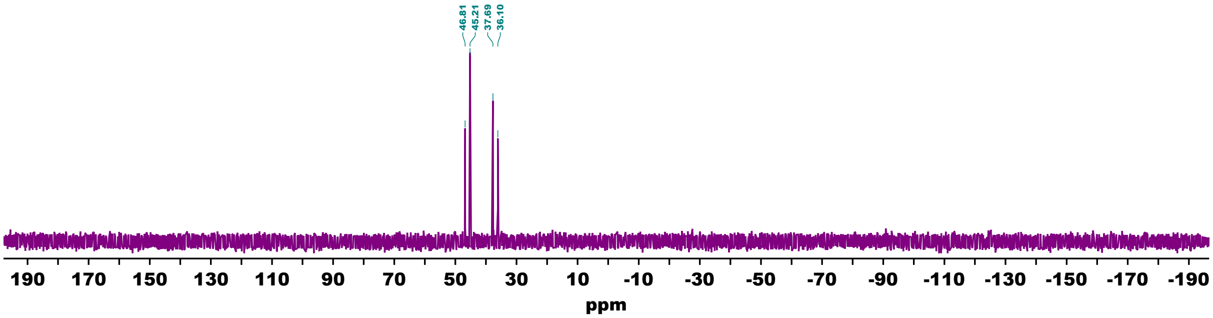

Figure S34. ^{31}P{^{1}H} NMR (162 MHz, DCM-d_2) spectrum of the *in situ* generated **[$^{\mathrm{L}}$Ir]$^{\mathrm{HB}}$**.

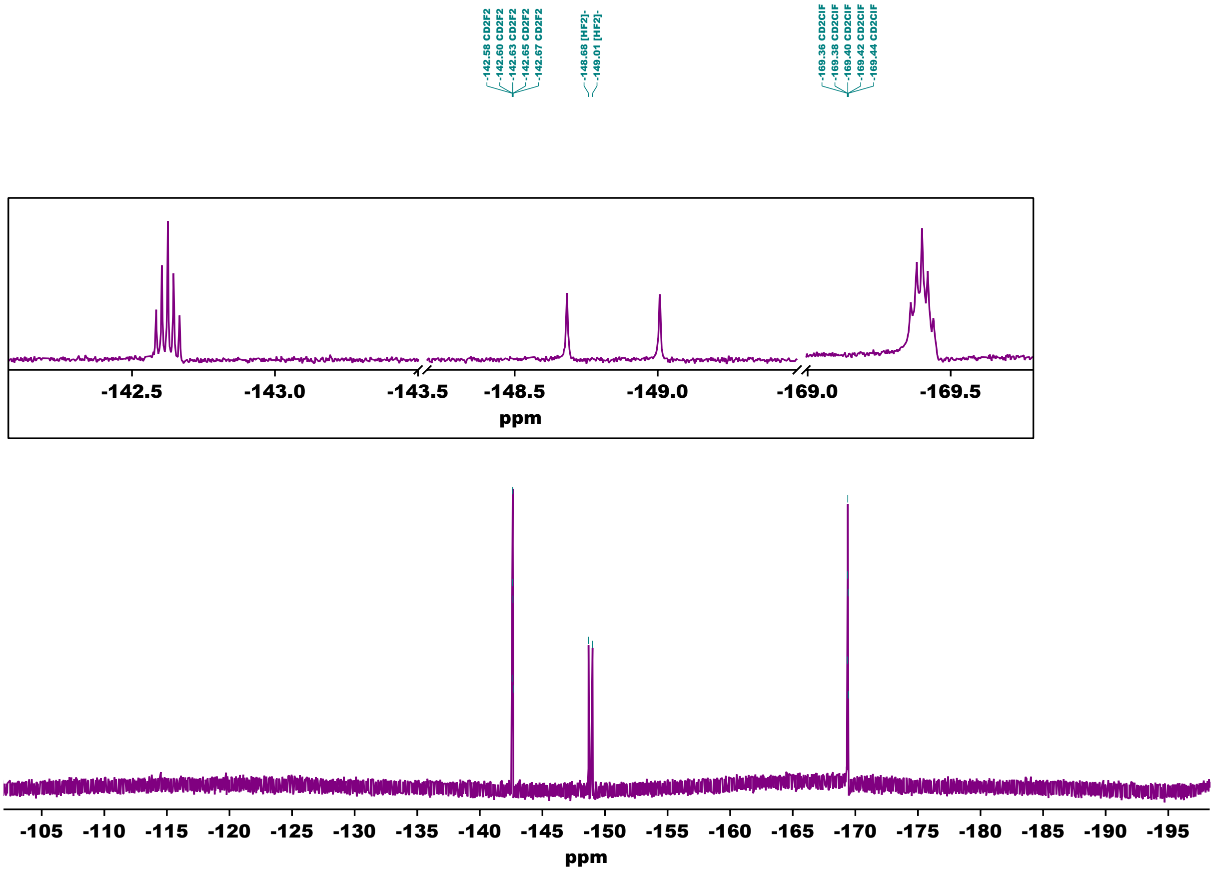

Figure S35. ^{19}F NMR (376 MHz, DCM-d_2) spectrum of the solution of **[$^{\mathrm{LH}}$Ir][F]** + 10 NMe$_4$F collected after a day of mixing.

Calculation of K_{eq} for the Overall Metal-Ligand Proton Tautomeric Equilibria of $[^{LH}Ir][X]$ Complexes (X = Cl, Br, I) in DCM-d_2

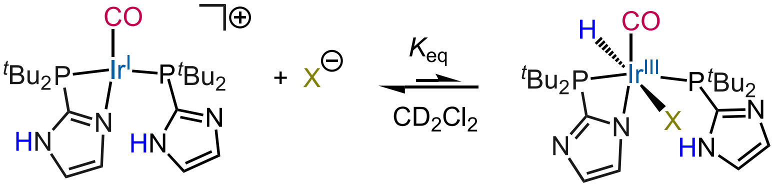

$[^{LH}Ir]$ $[X]$ $[H–^{L}Ir–X]$

Overall MLPT Equilbrium

As detailed in the manuscript (Scheme 1, A), the ligand-protonated $[^{LH}Ir][X]$ complexes (X = Cl, Br, I) equilibrate with their metal-protonated (or metal-hydridic) congeners **[H–^{L}Ir–X]** in solution (heating is required for Br and I to reach equilibrium stage). Accordingly, an expression for K_{eq} can be written as,

$$K_{eq} = \frac{conc.\,[H–^{L}Ir–X]}{conc.\,[^{LH}Ir] \times conc.\,[X]} \qquad …..(S1)$$

Since conc. **[^{LH}Ir]** = conc. **[X]**, the above expression in eq. (S1) can be rewritten as,

$$K_{eq} = \frac{conc.\,[H–^{L}Ir–X]}{(conc.\,[^{LH}Ir])^2} \qquad …..(S2)$$

To calculate K_{eq}, 1,3,5-trimethoxybenzene (TMB) was used as an internal standard (δ 6.07, 3.75 in DCM-d_2). The values for “conc. **[H–^{L}Ir–X]**” and “conc. **[^{LH}Ir]**” were determined *via* $^1H\{^{31}P\}$ NMR spectroscopy, relative to the internal standard.

The calculation of K_{eq} for one of the trials with the chloride complex (Entry 1, Table S1) is shown below. The K_{eq} for all other trials of the chloride as well as bromide and iodide complexes were determined in the same way.

- A standard solution of TMB was prepared by dissolving 4 mg TMB in 1.00 mL of DCM-d_2 (concentration = 0.023 M).
- A 0.45 mL DCM-d_2 solution of 6.7 mg solid **[^{LH}Ir][Cl]** was transferred to a J. Young tube, to which 0.10 mL of standard solution was also added (concentration of TMB in J. Young tube = (0.023*0.1)/0.55 = 0.0043 M).
- Thereafter, a $^1H\{^{31}P\}$ NMR spectrum of the resulting solution was collected (Figure S36). Setting the integral of the aromatic TMB resonance to 3.00 gave a concentration of

3.66*0.0043 M = 0.016 M for **[$^{\mathbf{LH}}$Ir]** and 0.47*0.0043 M = 0.002 M for **[H–$^{\mathbf{L}}$Ir–Cl]**. (The upfield hydride signal is characteristic for the **[H–$^{\mathbf{L}}$Ir–Cl]** species while the signal at δ 6.85 was deemed characteristic for the **[$^{\mathbf{LH}}$Ir]** cation – it was assumed to not contain any protons of **[H–$^{\mathbf{L}}$Ir–Cl]** because of its isolation, relative sharpness, and absence of any shoulders).

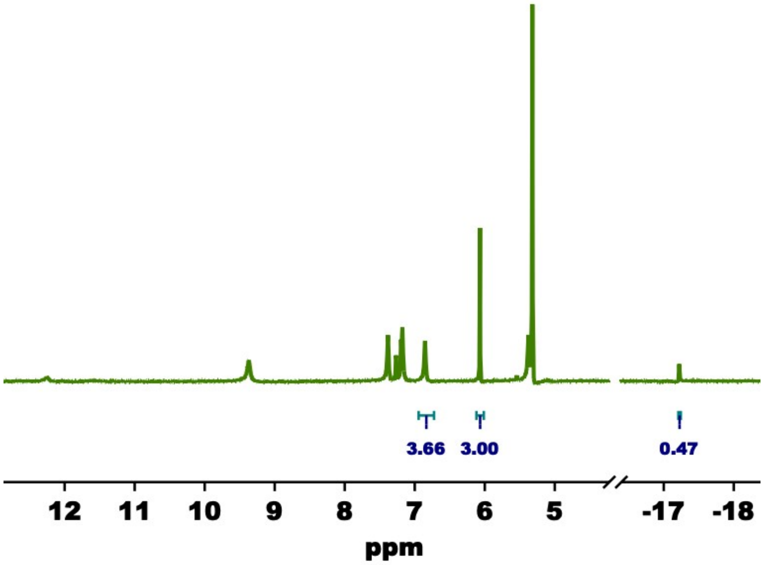

Figure S36. Partial ^{1}H{^{31}P} NMR spectrum (500 MHz) obtained after dissolving solid **[$^{\mathbf{LH}}$Ir][Cl]** in DCM-d_2 with TMB internal standard (δ 6.07).

- After obtaining the values of "conc. **[H–$^{\mathbf{L}}$Ir–Cl]**" and "conc. **[$^{\mathbf{LH}}$Ir]**", eq. S2 gave a K_{eq} value of 8.1 M^{-1}.

The tables showing values of "conc. **[H–$^{\mathbf{L}}$Ir–X]**", "conc. **[$^{\mathbf{LH}}$Ir]**", and K_{eq} for 3 different concentrations of each complex are shown below. The final K_{eq} values averaged over three trials are also provided. Note: Sonication to redissolve the crystalline products obtained under refluxing conditions (for bromide and iodide) might be required at periodic intervals until the equilibrium is attained.

Table S1. Calculation of K_{eq} for the chloride complex.

Entry	conc. [^{LH}Ir] (M)	conc. [H–^{L}Ir–Cl] (M)	K_{eq} (M^{-1})	Average K_{eq} (M^{-1})
1	1.6×10^{-2}	2.0×10^{-3}	8.1	8.4 ± 0.5
2	1.5×10^{-2}	1.8×10^{-3}	8.0	
3	1.4×10^{-2}	1.8×10^{-3}	9.1	

Table S2. Calculation of K_{eq} for the bromide complex.

Entry	conc. [^{LH}Ir] (M)	conc. [H–^{L}Ir–Br] (M)	K_{eq} (M^{-1})	Average K_{eq} (M^{-1})
1	8.9×10^{-3}	9.1×10^{-4}	11.5	10.6 ± 0.7
2	8.2×10^{-3}	6.7×10^{-4}	9.8	
3	7.4×10^{-3}	5.8×10^{-4}	10.5	

Table S3. Calculation of K_{eq} for the iodide complex.

Entry	conc. [^{LH}Ir] (M)	conc. [H–^{L}Ir–I] (M)	K_{eq} (M^{-1})	Average K_{eq} (M^{-1})
1	7.7×10^{-3}	1.2×10^{-3}	21.2	21.0 ± 0.3
2	6.2×10^{-3}	7.9×10^{-4}	20.5	
3	7.1×10^{-3}	1.1×10^{-3}	21.1	

X-Ray Crystallographic Data

[^{LH}Ir][Cl]

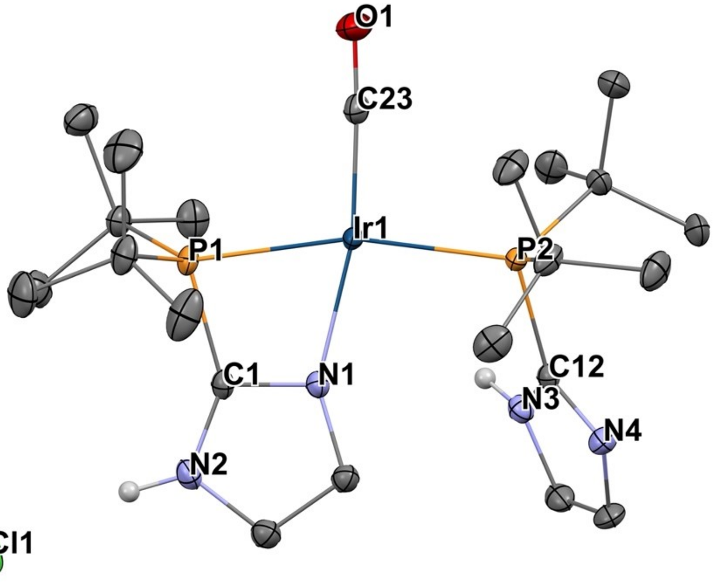

Bond	Distance (Å)
Ir1–P1	2.3318(4)
Ir1–P2	2.3169(4)
Ir1–N1	2.1128(14)
Ir1–C23	1.8161(18)
O1–C23	1.156(2)

Bonds	Angle (°)
P2–Ir1–P1	164.553(15)
N1–Ir1–P1	68.79(4)
C23–Ir1–N1	167.96(7)
C1–P1–Ir1	82.20(5)
C1–N1–Ir1	103.43(10)
N1–C1–P1	104.73(12)

Figure S37. Thermal ellipsoid plot of **[^{LH}Ir][Cl]** shown with 50% probability. H-atoms except for N–H's are omitted for clarity. Selected parameters shown at bottom.

Complex **[^{LH}Ir][Cl]**, $C_{23}H_{42}ClIrN_4OP_2$, crystallizes in the monoclinic space group $P2_1/c$ (systematic absences 0k0: k = odd and h0l: l = odd) with a = 17.5330(4) Å, b = 8.12170(10) Å, c = 21.3907(5) Å, β = 111.630(3)°, V = 2831.50(11) Å^3, Z = 4, and d_{calc} = 1.596 g/cm^3. X-ray intensity data were collected on a Rigaku XtaLAB Synergy-S diffractometer[7] equipped with an HPC area detector (Dectris Pilatus3 R 200K) and employing confocal multilayer optic-monochromated Mo-Kα radiation (λ = 0.71073 Å) at a temperature of 100 K. Preliminary indexing was performed from a series of thirty 0.5° rotation frames with exposures of 0.625 seconds. A total of 1656 frames (14 runs) were collected employing ω scans with a crystal to detector distance of 32.0 mm, rotation widths of 0.5° and exposures of 5 seconds. Rotation frames were integrated using CrysAlisPro,[7] producing a listing of unaveraged F^2 and $\sigma(F^2)$ values. A total of 84420 reflections were measured over the ranges $4.998 \leq 2\theta \leq 56.564°$, $-23 \leq h \leq 23$, $-9 \leq k \leq 10$, $-28 \leq l \leq 28$ yielding 7021 unique reflections ($R_{int} = 0.0459$). The intensity data were corrected for Lorentz and polarization effects and for absorption using SCALE3 ABSPACK[8] (minimum and maximum transmission 0.6260, 1.0000). The structure was solved by dual space methods - SHELXT v2014/4.[9] Refinement was by full-matrix least squares based on F^2 using SHELXL-2018.[10] All reflections were used during refinement. The weighting scheme used was $w = 1/[\sigma^2(F_o^2) + (0.0139P)^2 + 1.6915P]$ where $P = (F_o^2 + 2F_c^2)/3$. Non-hydrogen atoms were refined anisotropically and hydrogen atoms were refined using a riding model. Refinement converged to R1 = 0.0150 and wR2 = 0.0335 for 6532 observed reflections for which $F > 4\sigma(F)$ and R1 = 0.0172 and wR2 = 0.0340 and GOF = 1.032 for all 7021 unique, non-zero reflections and 301 variables. The maximum Δ/σ in the final cycle of least squares was 0.010 and the two most prominent peaks in the final difference Fourier were +0.83 and -0.43 e/Å^3.

Table S4. Summary of Structure Determination of [^{LH}Ir][Cl]

Empirical formula	$C_{23}H_{42}ClIrN_4OP_2$
Formula weight	680.19
CCDC number	2123873
Diffractometer	Rigaku XtaLAB Synergy-S
Temperature/K	100
Crystal system	monoclinic
Space group	$P2_1/c$
a	17.5330(4) Å
b	8.12170(10) Å
c	21.3907(5) Å
β	111.630(3)°
Volume	2831.50(11) Å^3
Z	4
d_{calc}	1.596 g/cm^3
μ	4.944 mm^{-1}
F(000)	1360.0
Crystal size, mm	0.15 × 0.1 × 0.02
2θ range for data collection	4.998 - 56.564°
Index ranges	$-23 \leq h \leq 23$, $-9 \leq k \leq 10$, $-28 \leq l \leq 28$
Reflections collected	84420
Independent reflections	7021 [R(int) = 0.0459]
Data/restraints/parameters	7021/0/301
Goodness-of-fit on F^2	1.032
Final R indexes [$I \geq 2\sigma(I)$]	$R_1 = 0.0150$, $wR_2 = 0.0335$
Final R indexes [all data]	$R_1 = 0.0172$, $wR_2 = 0.0340$
Largest diff. peak/hole	0.83/-0.43 eÅ^{-3}

Ir-1

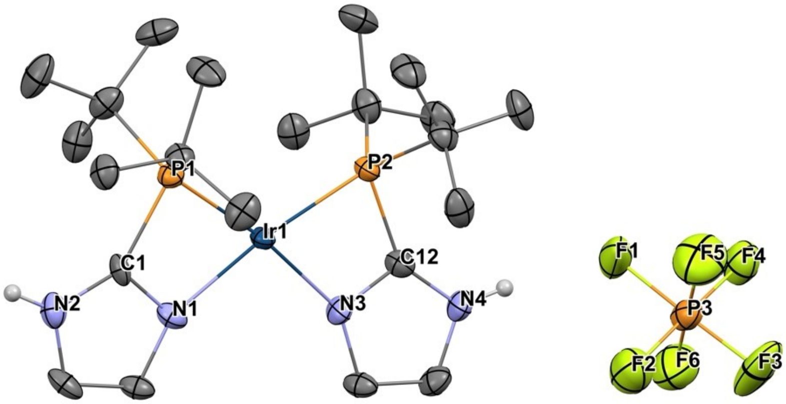

Bond	Distance (Å)
Ir1–P1	2.242(3)
Ir1–P2	2.256(2)
Ir1–N1	2.101(8)
Ir1–N3	2.083(8)

Bonds	Angle (°)
P1–Ir1–P2	117.74(9)
N1–Ir1–P1	70.4(2)
N1–Ir1–P2	171.8(2)
N3–Ir1–P1	172.1(2)
N3–Ir1–P2	70.1(2)
N3–Ir1–N1	101.8(3)

Figure S38. Thermal ellipsoid plot of **Ir-1** shown with 50% probability. H-atoms except for N–H's and co-crystallized solvent molecules are omitted for clarity. Selected parameters shown at bottom.

Complex **Ir-1** (+ 0.5 $CH_3C(O)CH_2C(OH)(CH_3)_2$), $C_{25}H_{48}F_6IrN_4OP_3$, crystallizes in the triclinic space group P**Error!**with a = 13.2443(2) Å, b = 16.1281(3) Å, c = 16.2491(3) Å, α = 77.4270(10)°, β = 82.2190(10)°, γ = 84.3570(10)°, V = 3347.95(10) Å^3, Z = 4, and d_{calc} = 1.626 g/cm^3. X-ray intensity data were collected on a Rigaku XtaLAB Synergy-S diffractometer[11] equipped with an HPC area detector (Dectris Pilatus3 R 200K) and employing confocal multilayer optic-monochromated Mo-Kα radiation (λ = 0.71073 Å) at a temperature of 100 K. Preliminary indexing was performed from a series of thirty 0.5° rotation frames with exposures of 1.25 seconds. A total of 1712 frames (14 runs) were collected employing ω scans with a crystal to detector distance of 34.0 mm, rotation widths of 0.5° and exposures of 15 seconds. Rotation frames were integrated using CrysAlisPro,[11] producing a listing of unaveraged F^2 and $\sigma(F^2)$ values. A total of 96516 reflections were measured over the ranges $4.834 \leq 2\theta \leq 56.564°$, $-17 \leq h \leq 17$, $-21 \leq k \leq 21$, $-21 \leq l \leq 21$ yielding 16564 unique reflections (R_{int} = 0.0621). The intensity data were corrected for

Lorentz and polarization effects and for absorption using SCALE3 ABSPACK[8] (minimum and maximum transmission 0.71532, 1.00000). The structure was solved by dual space methods - SHELXT.[9] Refinement was by full-matrix least squares based on F^2 using SHELXL-2018.[10] All reflections were used during refinement. The weighting scheme used was $w = 1/[\sigma^2(F_o^2) + (0.0482P)^2 + 81.8783P]$ where $P = (F_o^2 + 2F_c^2)/3$. Non-hydrogen atoms were refined anisotropically and hydrogen atoms were refined using a riding model. Refinement converged to R1 = 0.0649 and wR2 = 0.1615 for 12539 observed reflections for which $F > 4\sigma(F)$ and R1 = 0.0933 and wR2 = 0.1766 and GOF = 1.160 for all 16564 unique, non-zero reflections and 785 variables. The maximum Δ/σ in the final cycle of least squares was 0.001 and the two most prominent peaks in the final difference Fourier were +5.16 and -1.95 e/Å^3.

Table S5. Summary of Structure Determination of Ir-1

Empirical formula	$C_{25}H_{48}F_6IrN_4OP_3$
Formula weight	819.78
CCDC number	2123868
Diffractometer	Rigaku XtaLAB Synergy-S (Dectris Pilatus3 R 200K)
Temperature/K	100
Crystal system	triclinic
Space group	P**Error!**
a	13.2443(2) Å
b	16.1281(3) Å
c	16.2491(3) Å
α	77.4270(10)°
β	82.2190(10)°
γ	84.3570(10)°
Volume	3347.95(10) Å^3
Z	4
d_{calc}	1.626 g/cm^3
μ	4.190 mm^{-1}
F(000)	1640.0
Crystal size, mm	0.31 × 0.19 × 0.17
2θ range for data collection	4.834 - 56.564°
Index ranges	$-17 \leq h \leq 17$, $-21 \leq k \leq 21$, $-21 \leq l \leq 21$
Reflections collected	96516
Independent reflections	16564 [R(int) = 0.0621]
Data/restraints/parameters	16564/59/785
Goodness-of-fit on F^2	1.160
Final R indexes [$I \geq 2\sigma(I)$]	$R_1 = 0.0649$, $wR_2 = 0.1615$
Final R indexes [all data]	$R_1 = 0.0933$, $wR_2 = 0.1766$
Largest diff. peak/hole	5.16/-1.95 eÅ^{-3}

[$^{\mathbf{LH}}$Ir][PF$_6$]

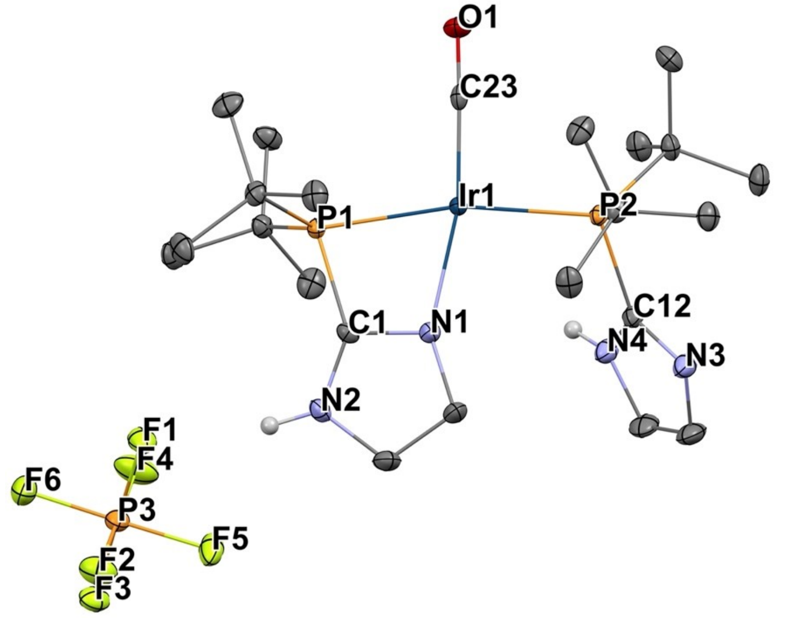

Bond	Distance (Å)
Ir1–P1	2.3379(5)
Ir1–P2	2.3251(5)
Ir1–N1	2.1351(18)
Ir1–C23	1.809(2)
O1–C23	1.160(3)

Bonds	Angle (°)
P2–Ir1–P1	165.040(18)
N1–Ir1–P1	68.95(4)
C23–Ir1–N1	167.87(8)
C1–P1–Ir1	82.05(7)
C1–N1–Ir1	102.37(13)
N1–C1–P1	106.63(14)

Figure S39. Thermal ellipsoid plot of **[$^{\mathbf{LH}}$Ir][PF$_6$]** shown with 50% probability. H-atoms except for N–H's are omitted for clarity. Selected parameters shown at bottom.

Complex **[$^{\mathbf{LH}}$Ir][PF$_6$]**, $C_{23}H_{42}F_6IrN_4OP_3$, crystallizes in the monoclinic space group $P2_1/c$ (systematic absences 0k0: k = odd and h0l: l = odd) with a = 12.0735(2) Å, b = 10.6615(2) Å, c = 23.5954(4) Å, β = 92.963(2)°, V = 3033.18(9) Å^3, Z = 4, and d_{calc} = 1.729 g/cm^3. X-ray intensity data were collected on a Rigaku XtaLAB Synergy-S[11] HPC area detector (Dectris Pilatus3 R 200K), employing confocal multilayer optic-monochromated Mo-Kα radiation (λ = 0.71073Å) at a temperature of 100 K. Preliminary indexing was performed from a series of thirty 0.5° rotation frames with exposures of 0.25 seconds. A total of 1116 frames (10 runs) were collected employing ω scans with a crystal to detector distance of 34.0 mm, rotation widths of 0.5° and exposures of 2 seconds. Rotation frames were integrated using CrysAlisPro,[11] producing a listing of unaveraged F^2 and $\sigma(F^2)$ values. A total of 58706 reflections were measured over the ranges $4.708 \leq 2\theta \leq 61.558°$, $-15 \leq h \leq 16$, $-15 \leq k \leq 12$, $-32 \leq l \leq 32$ yielding 8416 unique reflections ($R_{int} = 0.0449$). The intensity data were corrected for Lorentz and polarization effects and for absorption using SCALE3 ABSPACK[8] (minimum and maximum transmission 0.70006, 1.00000). The structure was solved by dual space methods - SHELXT.[9] Refinement was by full-matrix least squares based on F^2 using SHELXL-2018.[10] All reflections were used during refinement. The weighting scheme used was $w = 1/[\sigma^2(F_o^2) + (0.0216P)^2 + 0.4746P]$ where $P = (F_o^2 + 2F_c^2)/3$. Non-hydrogen atoms were refined anisotropically and hydrogen atoms were refined using a riding model. Refinement converged to R1 = 0.0206 and wR2 = 0.0452 for 7357 observed reflections for which $F > 4\sigma(F)$ and R1 = 0.0280 and wR2 = 0.0467 and GOF = 1.081 for all 8416 unique, non-zero reflections and 355 variables. The maximum Δ/σ in the final cycle of least squares was 0.004 and the two most prominent peaks in the final difference Fourier were +1.01 and -0.84 e/Å^3.

Table S6. Summary of Structure Determination of [^{LH}Ir][PF$_6$]

Empirical formula	$C_{23}H_{42}F_6IrN_4OP_3$
Formula weight	789.71
CCDC number	2123870
Temperature/K	100
Crystal system	monoclinic
Space group	$P2_1/c$
a	12.0735(2) Å
b	10.6615(2) Å
c	23.5954(4) Å
β	92.963(2)°
Volume	3033.18(9) Å^3
Z	4
d_{calc}	1.729 g/cm^3
μ	4.621 mm^{-1}
F(000)	1568.0
Crystal size, mm	0.27 × 0.12 × 0.11
2θ range for data collection	4.708 - 61.558°
Index ranges	$-15 \leq h \leq 16$, $-15 \leq k \leq 12$, $-32 \leq l \leq 32$
Reflections collected	58706
Independent reflections	8416 [R(int) = 0.0449]
Data/restraints/parameters	8416/0/355
Goodness-of-fit on F^2	1.081
Final R indexes [$I \geq 2\sigma$ (I)]	$R_1 = 0.0206$, $wR_2 = 0.0452$
Final R indexes [all data]	$R_1 = 0.0280$, $wR_2 = 0.0467$
Largest diff. peak/hole	1.01/-0.84 eÅ^{-3}

$[^{LH}Ir][Br]$

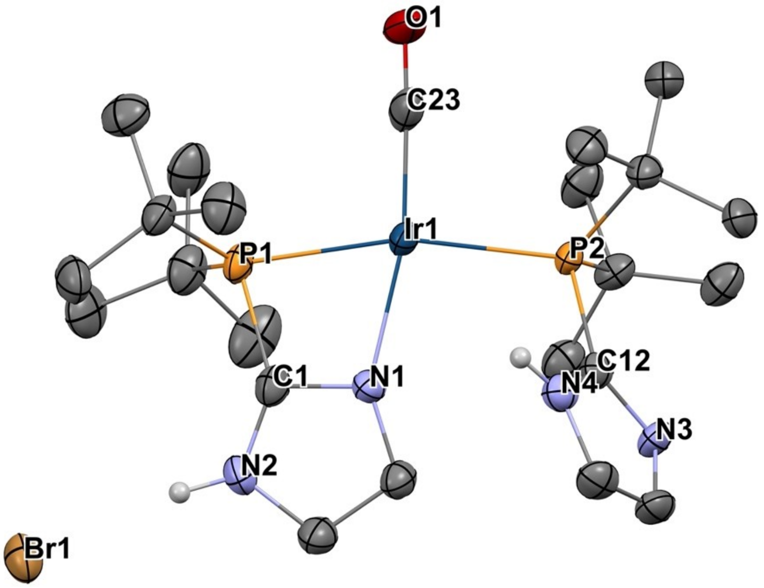

Bond	Distance (Å)
Ir1–P1	2.3363(12)
Ir1–P2	2.3166(12)
Ir1–N1	2.125(4)
Ir1–C23	1.809(6)
O1–C23	1.156(7)

Bonds	Angle (°)
P2–Ir1–P1	164.68(4)
N1–Ir1–P1	68.81(12)
C23–Ir1–N1	168.0(2)
C1–P1–Ir1	82.32(17)
C1–N1–Ir1	103.1(3)
N1–C1–P1	105.0(4)

Figure S40. Thermal ellipsoid plot of **$[^{LH}Ir][Br]$** shown with 50% probability. H-atoms except for N–H's are omitted for clarity. Selected parameters shown at bottom.

Complex **$[^{LH}Ir][Br]$**, $C_{23}H_{42}BrIrN_4OP_2$, crystallizes in the monoclinic space group $P2_1/c$ (systematic absences 0k0: k = odd and h0l: l = odd) with a = 17.7005(4) Å, b = 8.11750(10) Å, c = 21.3840(4) Å, β = 111.189(2)°, V = 2864.81(10) Å^3, Z = 4, and d_{calc}= 1.680 g/cm^3 . X-ray intensity data were collected on a Rigaku XtaLAB Synergy-S diffractometer[11] equipped with an HPC area detector (HyPix-6000HE) and employing confocal multilayer optic-monochromated Cu-Kα radiation (λ = 1.54184 Å) at a temperature of 100 K. Preliminary indexing was performed from a series of sixty 0.5° rotation frames with exposures of 1.25 sec. at θ = ± 48.77° and 5 sec. at θ=105.75°. A total of 4500 frames (49 runs) were collected employing ω scans with a crystal to detector distance of 31.6 mm, rotation widths of 0.5° and exposures of 3 seconds at θ = ±48.77°, 12 seconds at θ = -84.25° and θ = 105.75°. Rotation frames were integrated using CrysAlisPro,[11] producing a listing of unaveraged F^2 and $\sigma(F^2)$ values. A total of 44440 reflections were measured over the ranges $5.354 \leq 2\theta \leq 149.002°$, $-22 \leq h \leq 21$, $-9 \leq k \leq 10$, $-26 \leq l \leq 20$ yielding 5853 unique reflections (R_{int} = 0.0770). The intensity data were corrected for Lorentz and polarization effects and for absorption using SCALE3 ABSPACK[8] (minimum and maximum transmission 0.4993, 1.0000). The structure was solved by duals space methods - SHELXT.[9] Refinement was by full-matrix least squares based on F^2 using SHELXL-2018.[10] All reflections were used during refinement. The weighting scheme used was $w = 1/[\sigma^2(F_o^2) + (0.0671P)^2 + 6.1235P]$ where $P = (F_o^2 + 2F_c^2)/3$. Non-hydrogen atoms were refined anisotropically and hydrogen atoms were refined using a riding model. Refinement converged to R1 = 0.0397 and wR2 = 0.1120 for 5235 observed reflections for which $F > 4\sigma(F)$ and R1 = 0.0437 and wR2 = 0.1145 and GOF = 1.121 for all 5853 unique, non-zero reflections and 301 variables. The maximum Δ/σ in the final cycle of least squares was 0.000 and the two most prominent peaks in the final difference Fourier were +1.04 and -2.37 e/Å^3.

Table S7. Summary of Structure Determination of $[^{LH}Ir][Br]$

Empirical formula	$C_{23}H_{42}BrIrN_4OP_2$
Formula weight	724.65
CCDC number	2123869
Diffractometer	Rigaku XtaLAB Synergy-S
Temperature/K	100(2)
Crystal system	monoclinic
Space group	$P2_1/c$
a	17.7005(4) Å
b	8.11750(10) Å
c	21.3840(4) Å
β	111.189(2)°
Volume	2864.81(10) $Å^3$
Z	4
d_{calc}	1.680 g/cm^3
μ	11.875 mm^{-1}
F(000)	1432.0
Crystal size, mm	0.17 × 0.03 × 0.01
2θ range for data collection	5.354 - 149.002°
Index ranges	$-22 \le h \le 21$, $-9 \le k \le 10$, $-26 \le l \le 20$
Reflections collected	44440
Independent reflections	5853 [R(int) = 0.0770]
Data/restraints/parameters	5853/0/301
Goodness-of-fit on F^2	1.121
Final R indexes [$I \ge 2\sigma(I)$]	$R_1 = 0.0397$, $wR_2 = 0.1120$
Final R indexes [all data]	$R_1 = 0.0437$, $wR_2 = 0.1145$

[$^{\mathbf{LH}}$Ir][I]

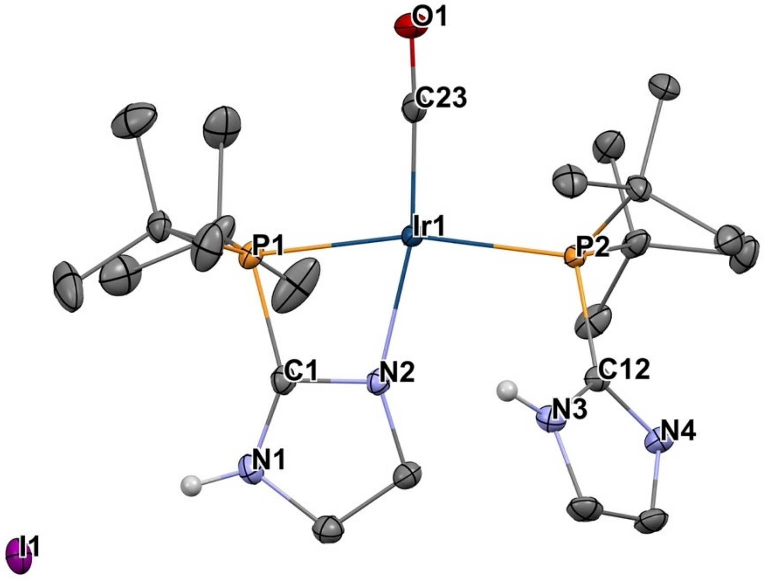

Bond	Distance (Å)
Ir1–P1	2.3367(6)
Ir1–P2	2.3171(6)
Ir1–N2	2.123(2)
Ir1–C23	1.817(3)
O1–C23	1.156(3)

Bonds	Angle (°)
P2–Ir1–P1	164.84(2)
N2–Ir1–P1	68.89(6)
C23–Ir1–N2	168.06(10)
C1–P1–Ir1	82.05(8)
C1–N2–Ir1	102.88(15)
N2–C1–P1	105.51(17)

Figure S41. Thermal ellipsoid plot of **[$^{\mathbf{LH}}$Ir][I]** shown with 50% probability. H-atoms except for N–H's are omitted for clarity. Selected parameters shown at bottom.

Complex **[$^{\mathbf{LH}}$Ir][I]**, $C_{23}H_{42}IIrN_4OP_2$, crystallizes in the monoclinic space group $P2_1/c$ (systematic absences 0k0: k = odd and h0l: l = odd) with a =17.9499(6) Å, b = 8.1504(2) Å, c = 21.5003(8) Å, β = 110.968(4)°, V = 2937.18(18) Å^3, Z = 4, and d_{calc} =1.745 g/cm^3. X-ray intensity data were collected on a Rigaku XtaLAB Synergy-S diffractometer[7] equipped with an HPC area detector (Dectris Pilatus3 R 200K) and employing confocal multilayer optic-monochromated Mo-Kα radiation (λ=0.71073 Å) at a temperature of 100 K. Preliminary indexing was performed from a series of thirty 0.5° rotation frames with exposures of 2.5 seconds. A total of 1456 frames (11 runs) were collected employing ω scans with a crystal to detector distance of 40.0 mm, rotation widths of 0.5° and exposures of 10 seconds. Rotation frames were integrated using CrysAlisPro,[7] producing a listing of unaveraged F^2 and $\sigma(F^2)$ values. A total of 57828 reflections were measured over the ranges $4.86 \leq 2\theta \leq 56.562°$, $-23 \leq h \leq 23$, $-10 \leq k \leq 10$, $-28 \leq l \leq 28$ yielding 7274 unique reflections ($R_{int} = 0.0484$). The intensity data were corrected for Lorentz and polarization effects and for absorption using SCALE3 ABSPACK[8] (minimum and maximum transmission 0.5448, 1.0000). The structure was solved by dual space methods - SHELXT.[9] Refinement was by full-matrix least squares based on F^2 using SHELXL-2018.[10] All reflections were used during refinement. The weighting scheme used was $w = 1/[\sigma^2(F_o^2) + (0.0205P)^2 + 2.2249P]$ where $P = (F_o^2 + 2F_c^2)/3$. Non-hydrogen atoms were refined anisotropically and hydrogen atoms were refined using a riding model. Refinement converged to $R1 = 0.0216$ and $wR2 = 0.0465$ for 6523 observed reflections for which $F > 4\sigma(F)$ and $R1 = 0.0267$ and $wR2 = 0.0477$ and $GOF = 1.041$ for all 7274 unique, non-zero reflections and 301 variables. The maximum Δ/σ in the final cycle of least squares was 0.003 and the two most prominent peaks in the final difference Fourier were +0.84 and -0.87 e/Å^3.

Table S8. Summary of Structure Determination of [^{LH}Ir][I]

Empirical formula	$C_{23}H_{42}IIrN_4OP_2$
Formula weight	771.64
CCDC number	2123871
Diffractometer	Rigaku XtaLAB Synergy-S
Temperature/K	100
Crystal system	monoclinic
Space group	$P2_1/c$
a	17.9499(6) Å
b	8.1504(2) Å
c	21.5003(8) Å
β	110.968(4)°
Volume	2937.18(18) Å^3
Z	4
d_{calc}	1.745 g/cm^3
μ	5.727 mm^{-1}
F(000)	1504.0
Crystal size, mm	0.25 × 0.11 × 0.02
2θ range for data collection	4.86 - 56.562°
Index ranges	$-23 \leq h \leq 23$, $-10 \leq k \leq 10$, $-28 \leq l \leq 28$
Reflections collected	57828
Independent reflections	7274 [R(int) = 0.0484]
Data/restraints/parameters	7274/0/301
Goodness-of-fit on F^2	1.042
Final R indexes [$I \geq 2\sigma(I)$]	$R_1 = 0.0216$, $wR_2 = 0.0465$
Final R indexes [all data]	$R_1 = 0.0267$, $wR_2 = 0.0477$
Largest diff. peak/hole	0.84/-0.87 eÅ^{-3}

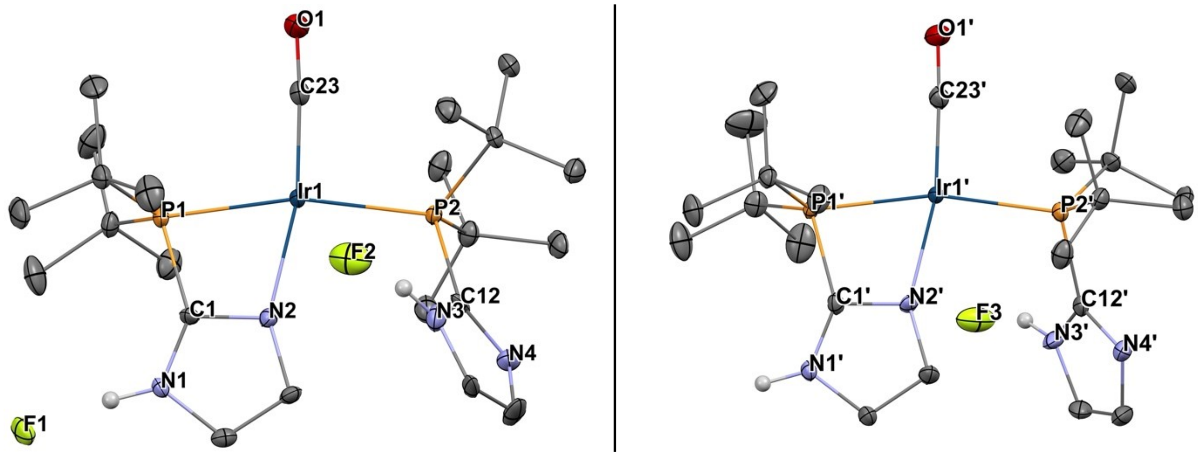

[$^{\mathrm{LH}}$Ir][F]

Bond	**Distance (Å)**	**Bond**	**Distance (Å)**
Ir1–P1	2.3368(18)	Ir1'–P1'	2.3224(18)
Ir1–P2	2.3308(18)	Ir1'–P2'	2.3119(18)
Ir1–N2	2.110(6)	Ir1'–N2'	2.110(6)
Ir1–C23	1.814(8)	Ir1'–C23'	1.813(8)
O1–C23	1.155(10)	O1'–C23'	1.159(10)

Bonds	**Angle (°)**	**Bonds**	**Angle (°)**
P2–Ir1–P1	165.42(6)	P2'–Ir1'–P1'	165.43(6)
N2–Ir1–P1	68.82(17)	N2'–Ir1'–P1'	69.16(17)
C23–Ir1–N2	167.8(3)	C23'–Ir1'–N2'	167.8(3)
C1–P1–Ir1	82.1(2)	C1'–P1'–Ir1'	82.3(2)
C1–N2–Ir1	102.9(4)	C1'–N2'–Ir1'	102.9(4)
N2–C1–P1	105.7(5)	N2'–C1'–P1'	105.2(5)

Figure S42. Thermal ellipsoid plot of **[$^{\mathrm{LH}}$Ir][F]**'s asymmetric unit 1 (left) and asymmetric unit 2 (right) shown with 50% probability. H-atoms except for N–H's and co-crystallized solvent molecules are omitted for clarity. Selected parameters shown at bottom.

Complex **[$^{\mathrm{LH}}$Ir][F]** (+ **[$^{\mathrm{LH}}$Ir][F]** + H_2O + CH_3CN), $C_{48}H_{89}F_2Ir_2N_9O_3P_4$, crystallizes in the triclinic space group P**Error!**with a = 11.8995(2) Å, b = 16.0723(2) Å, c = 17.0807(2) Å, α = 67.2030(10)°,

β = 75.2190(10)°, γ = 89.3060(10)°, V = 2898.06(7) Å^3, Z = 2, and d_{calc} =1.589 g/cm^3. X-ray intensity data were collected on a Rigaku XtaLAB Synergy-S diffractometer[7] equipped with an HPC area detector (HyPix-6000HE) and employing confocal multilayer optic-monochromated Mo-Kα radiation (λ = 0.71073 Å) at a temperature of 100 K. Preliminary indexing was performed from a series of thirty 0.5° rotation frames with exposures of 0.25 seconds. A total of 2342 frames (12 runs) were collected employing ω scans with a crystal to detector distance of 42.0 mm, rotation widths of 0.5° and exposures of 5 seconds. Rotation frames were integrated using CrysAlisPro,[7] producing a listing of unaveraged F^2 and $\sigma(F^2)$ values. A total of 87784 reflections were measured over the ranges $3.556 \leq 2\theta \leq 56.564°$, $-15 \leq h \leq 15$, $-21 \leq k \leq 21$, $-22 \leq l \leq 22$ yielding 14362 unique reflections (R_{int} = 0.0454). The intensity data were corrected for Lorentz and polarization effects and for absorption using SCALE3 ABSPACK[8] (minimum and maximum transmission 0.6817, 1.0000). The structure was solved by dual space methods - SHELXT.[9] The first solution of the structure seemed to show three F^{-} ions, but two had rather slightly larger thermal parameters. It was hypothesized that these two positions were occupied by a F^{-} ion in half of the asymmetric units and by oxygen atoms of water molecules in the other half. Thus, F2 and F3 in Figure S42 are actually 50/50 mixtures of F and O. Refinement was by full-matrix lea squares based on F^2 using SHELXL-2018.[10] All reflections were used during refinement. The weighting scheme used was $w = 1/[\sigma^2(F_o^2) + 49.9701P]$ where $P = (F_o^2 + 2F_c^2)/3$. Non-hydrogen atoms were refined anisotropically and hydrogen atoms were refined using a riding model. Refinement converged to R1 = 0.0461 and wR2 = 0.1235 for 13222 observed reflections for which $F > 4\sigma(F)$ and R1 = 0.0508 and wR2 = 0.1246 and GOF = 1.358 for all 14362 unique, non-zero reflections and 638 variables. The maximum Δ/σ in the final cycle of least squares was 0.001 and the two most prominent peaks in the final difference Fourier were +3.32 and -2.49 e/Å^3.

Table S9. Summary of Structure Determination of $[^{LH}Ir][F]$

Empirical formula	$C_{48}H_{89}F_2Ir_2N_9O_3P_4$
Formula weight	1386.56
CCDC number	2123872
Diffractometer	Rigaku XtaLAB Synergy-S
Temperature/K	100(2)
Crystal system	triclinic
Space group	P**Error!**
a	11.8995(2) Å
b	16.0723(2) Å
c	17.0807(2) Å
α	67.2030(10)°
β	75.2190(10)°
γ	89.3060(10)°
Volume	2898.06(7) $Å^3$
Z	2
d_{calc}	1.589 g/cm^3
μ	4.750 mm^{-1}
F(000)	1392.0
Crystal size, mm	0.12 × 0.08 × 0.07
2θ range for data collection	3.556 - 56.564°
Index ranges	$-15 \le h \le 15$, $-21 \le k \le 21$, $-22 \le l \le 22$
Reflections collected	87784
Independent reflections	14362 [R(int) = 0.0454]
Data/restraints/parameters	14362/0/638
Goodness-of-fit on F^2	1.358

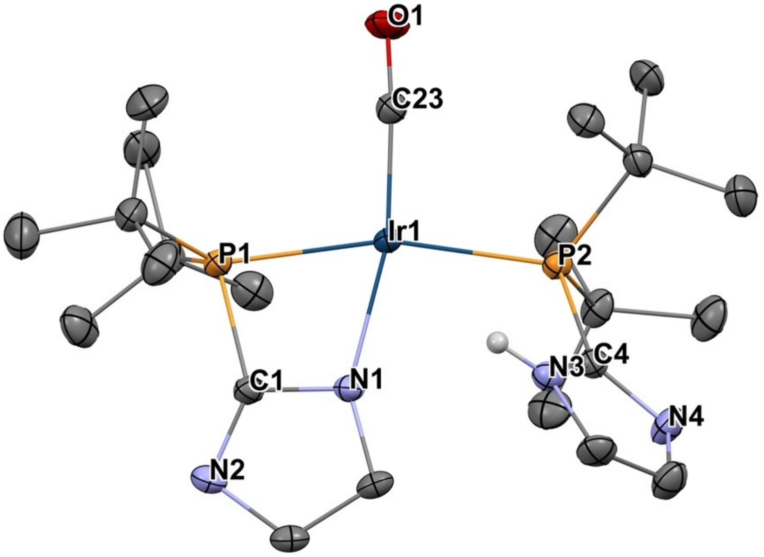

[^{L}Ir]

Bond	Distance (Å)
Ir1–P1	2.3326(13)
Ir1–P2	2.3238(12)
Ir1–N1	2.094(4)
Ir1–C23	1.821(5)
O1–C23	1.153(6)

Bonds	Angle (°)
P2–Ir1–P1	163.55(4)
N1–Ir1–P1	68.76(11)
C23–Ir1–N1	166.94(19)
C1–P1–Ir1	83.04(16)
C1–N1–Ir1	104.4(3)
N1–C1–P1	103.8(3)

Figure S43. Thermal ellipsoid plot of **[^{L}Ir]** (only 1 asymmetric unit out of 3) shown with 50% probability. H-atoms except for N–H's and co-crystalized solvent molecules are omitted for clarity. Selected parameters shown at bottom.

Complex **[^{L}Ir]** (+ 1.5 CH_3CN), $C_{26}H_{45.5}IrN_{5.5}OP_2$, crystallizes in the orthorhombic space group Pbca (systematic absences h0l: h = odd and 0kl: k + l = odd) with a = 26.01830(10) Å, b = 23.43300(10) Å, c = 31.3406(2)Å, V = 19107.95(16) Å^3, Z = 24, and d_{calc} =1.471 g/cm^3. X-ray intensity data were collected on a Rigaku XtaLAB Synergy-S diffractometer[7] equipped with an HPC area detector (HyPix-6000HE) and employing confocal multilayer optic-monochromated Mo-Kα radiation (λ =0.71073 Å) at a temperature of 100 K. Preliminary indexing was performed from a series of thirty 0.5° rotation frames with exposures of 0.625 seconds. A total of 2770 frames (13 runs) were collected employing ω scans with a crystal to detector distance of 50.0 mm, rotation widths of 0.5° and exposures of 10 seconds. Rotation frames were integrated using CrysAlisPro,[7] producing a listing of unaveraged F^2 and $\sigma(F^2)$ values. A total of 563209 reflections were measured over the ranges $3.476 \leq 2\theta \leq 56.654°$, $-34 \leq h \leq 34$, $-31 \leq k \leq 31$, $-41 \leq l \leq 41$ yielding 23761 unique reflections ($R_{int} = 0.0529$). The intensity data were corrected for Lorentz and polarization effects and for absorption using SCALE3 ABSPACK[8] (minimum and maximum transmission 0.6046, 1.0000). The structure was solved by dual space methods - SHELXT.[9] Refinement was by full-matrix least squares based on F^2 using SHELXL-2018.[10] All reflections were used during refinement. The weighting scheme used was $w = 1/[\sigma^2(F_o^2) + (0.0299P)^2 + 118.6224P]$ where $P = (F_o^2 + 2F_c^2)/3$. Non-hydrogen atoms were refined anisotropically and hydrogen atoms were refined using a riding model. Refinement converged to R1 = 0.0394 and wR2 = 0.0979 for 21647 observed reflections for which $F > 4\sigma(F)$ and R1 = 0.0449 and wR2 = 0.0996 and GOF = 1.265 for all 23761 unique, non-zero reflections and 994 variables. The maximum Δ/σ in the final cycle of least squares was 0.003 and the two most prominent peaks in the final difference Fourier were +2.50 and -1.30 e/Å^3.

Table S10. Summary of Structure Determination of [$^{\mathrm{L}}$Ir]

Empirical formula	$C_{26}H_{45.5}IrN_{5.5}OP_2$
Formula weight	705.32
CCDC number	2123867
Diffractometer	Rigaku XtaLAB Synergy-S
Temperature/K	100(2)
Crystal system	orthorhombic
Space group	Pbca
a	26.01830(10) Å
b	23.43300(10) Å
c	31.3406(2) Å
Volume	19107.95(16) Å^3
Z	24
d_{calc}	1.471 g/cm^3
μ	4.319 mm^{-1}
F(000)	8520.0
Crystal size, mm	0.18 × 0.12 × 0.06
2θ range for data collection	3.476 - 56.654°
Index ranges	$-34 \leq h \leq 34$, $-31 \leq k \leq 31$, $-41 \leq l \leq 41$
Reflections collected	563209
Independent reflections	23761 [R(int) = 0.0529]
Data/restraints/parameters	23761/123/994
Goodness-of-fit on F^2	1.265
Final R indexes [I ≥ 2σ (I)]	$R_1 = 0.0394$, $wR_2 = 0.0979$
Final R indexes [all data]	$R_1 = 0.0449$, $wR_2 = 0.0996$
Final R indexes [all data]	$R_1 = 0.0437$, $wR_2 = 0.1145$

Ir-2

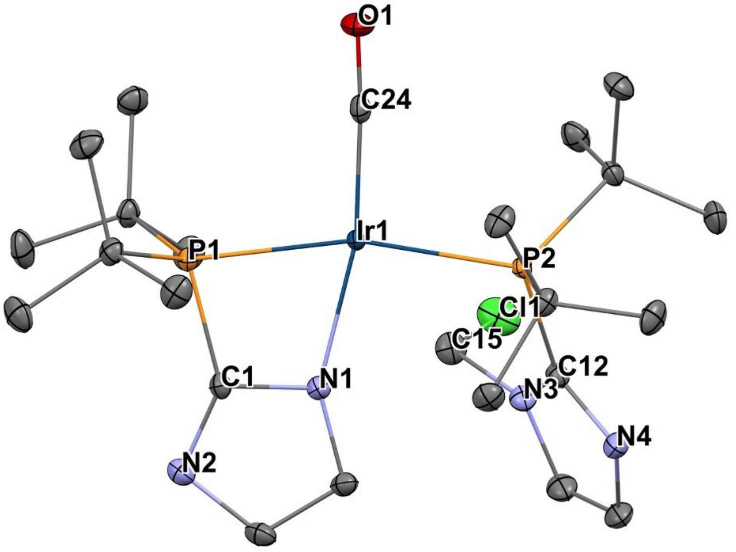

Bond	Distance (Å)
Ir1–P1	2.3379(4)
Ir1–P2	2.3209(4)
Ir1–N1	2.1016(15)
Ir1–C24	1.8109(19)
O1–C24	1.161(2)

Bonds	Angle (°)
P2–Ir1–P1	164.153(16)
N1–Ir1–P1	68.69(4)
C24–Ir1–N1	167.79(7)
C1–P1–Ir1	82.98(6)
C1–N1–Ir1	103.95(11)
N1–C1–P1	104.07(12)

Figure S44. Thermal ellipsoid plot of **Ir-2** shown with 50% probability. H-atoms and co-crystalized solvent molecules are omitted for clarity. Selected parameters shown at bottom.

Complex **Ir-2** (+ CH_2Cl_2), $C_{25}H_{44}Cl_3IrN_4OP_2$, crystallizes in the monoclinic space group $P2_1/n$ (systematic absences 0k0: k = odd and h0l: h + l = odd) with a = 11.94450(10) Å, b = 10.19850(10) Å, c = 25.8721(3) Å, β = 94.0160(10)°, V = 3143.90(5) Å^3, Z = 4, and d_{calc} =1.642 g/cm^3. X-ray intensity data were collected on a Rigaku XtaLAB Synergy-S diffractometer[12] equipped with an HPC area detector (HyPix-6000HE) and employing confocal multilayer optic-monochromated Mo-Kα radiation (λ=0.71073 Å) at a temperature of 100 K. Preliminary indexing was performed from a series of thirty 0.5° rotation frames with exposures of 0.25 seconds. A total of 1358 frames (13 runs) were collected employing ω scans with a crystal to detector distance of 34.0 mm, rotation widths of 0.5° and exposures of 1 seconds. Rotation frames were integrated using CrysAlisPro,[12] producing a listing of unaveraged F^2 and $\sigma(F^2)$ values. A total of 67574 reflections were measured over the ranges $3.664 \leq 2\theta \leq 56.564°$, $-15 \leq h \leq 15$, $-13 \leq k \leq 13$, $-34 \leq l \leq 34$ yielding 7805 unique reflections ($R_{int} = 0.0352$). The intensity data were corrected for Lorentz and polarization effects and for absorption using SCALE3 ABSPACK[8] (minimum and maximum transmission 0.7606, 1.0000). The structure was solved by dual space methods - SHELXT.[9] Refinement was by full-matrix least squares based on F^2 using SHELXL.[10] All reflections were used during refinement. The weighting scheme used was $w = 1/[\sigma^2(F_o^2) + (0.0061P)^2 + 3.6611P]$ where $P = (F_o^2 + 2F_c^2)/3$. Non-hydrogen atoms were refined anisotropically and hydrogen atoms were refined using a riding model. Refinement converged to R1 = 0.0163 and wR2 = 0.0335 for 7369 observed reflections for which $F > 4\sigma(F)$ and R1 = 0.0182 and wR2 = 0.0340 and GOF = 1.074 for all 7805 unique, non-zero reflections and 337 variables. The maximum Δ/σ in the final cycle of least squares was 0.003 and the two most prominent peaks in the final difference Fourier were +1.15 and -0.78 e/Å^3.

Table S11. Summary of Structure Determination of Compound Ir-2

Empirical formula	$C_{25}H_{44}Cl_3IrN_4OP_2$
Formula weight	777.13
CCDC number	2123874
Diffractometer	Rigaku XtaLAB Synergy-S (HyPix-6000HE)
Temperature/K	100
Crystal system	monoclinic
Space group	$P2_1/n$
a	11.94450(10) Å
b	10.19850(10) Å
c	25.8721(3) Å
β	94.0160(10)°
Volume	3143.90(5) $Å^3$
Z	4
d_{calc}	1.642 g/cm^3
μ	4.629 mm^{-1}
F(000)	1552.0
Crystal size, mm	0.27 × 0.22 × 0.2
2θ range for data collection	3.664 - 56.564°
Index ranges	$-15 \leq h \leq 15$, $-13 \leq k \leq 13$, $-34 \leq l \leq 34$
Reflections collected	67574
Independent reflections	7805 [R(int) = 0.0352]
Data/restraints/parameters	7805/0/337
Goodness-of-fit on F^2	1.074
Final R indexes [$I \geq 2\sigma (I)$]	$R_1 = 0.0163$, $wR_2 = 0.0335$
Final R indexes [all data]	$R_1 = 0.0182$, $wR_2 = 0.0340$
Largest diff. peak/hole	1.15/-0.78 $eÅ^{-3}$

References

1 J. L. Herde, J. C. Lambert, C. V. Senoff and M. A. Cushing, *Inorg. Synth.,* 1974, **15**, 18-20.

2 D. B. Grotjahn, Y. Gong, A. G. DiPasquale, L. N. Zakharov and A. L. Rheingold, *Organometallics,* 2006, **25**, 5693-5695.

3 R. Dorta, R. Goikhman and D. Milstein, *Organometallics,* 2003, **22**, 2806-2809.

4 G. R. Fulmer, A. J. M. Miller, N. H. Sherden, H. E. Gottlieb, A. Nudelman, B. M. Stoltz, J. E. Bercaw and K. I. Goldberg, *Organometallics,* 2010, **29**, 2176-2179.

5 V. V. Grushin, *Angew. Chem. Int. Ed.,* 1998, **37**, 994-996.

6 K. O. Christe and W. W. Wilson, *J. Fluor. Chem.,* 1990, **47**, 117-120.

7 CrysAlisPro 1.171.40.84a: Rigaku Oxford Diffraction, Rigaku Corporation, Oxford, UK, 2020.

8 SCALE3 ABSPACK v1.0.7: an Oxford Diffraction program; Oxford Diffraction Ltd: Abingdon, UK, 2005.

9 SHELXT v2014/4: G. M. Sheldrick, *Acta Cryst.,* 2015, **A71**, 3-8.

10 SHELXL-2018/3: G. M. Sheldrick, *Acta Cryst.,* 2015, **A71**, 3-8.

11 CrysAlisPro 1.171.40.53: Rigaku Oxford Diffraction, Rigaku Corporation, Oxford, UK, 2019.

12 CrysAlisPro 1.171.41.115a: Rigaku Oxford Diffraction, Rigaku Corporation, Oxford, UK, 2021.